creative commons
COMMONS DEED

저작자표시-비영리 2.0 대한민국

이용자는 아래의 조건을 따르는 경우에 한하여 자유롭게

- 이 저작물을 복제, 배포, 전송, 전시, 공연 및 방송할 수 있습니다.
- 이차적 저작물을 작성할 수 있습니다.

다음과 같은 조건을 따라야 합니다:

저작자표시. 귀하는 원저작자를 표시하여야 합니다.

비영리. 귀하는 이 저작물을 영리 목적으로 이용할 수 없습니다.

- 귀하는, 이 저작물의 재이용이나 배포의 경우, 이 저작물에 적용된 이용허락조건을 명확하게 나타내어야 합니다.
- 저작권자로부터 별도의 허가를 받으면 이러한 조건들은 적용되지 않습니다.

저작권법에 따른 이용자의 권리는 위의 내용에 의하여 영향을 받지 않습니다.

이것은 이용허락규약(Legal Code)을 이해하기 쉽게 요약한 것입니다.

Disclaimer

dCollection

공학석사 학위논문

Design of SFR Vortex-type Fluidic Diode Port using Topology Optimization and Computational Fluid Dynamics Simulation

위상최적화 및 전산유체해석을 활용한 Vortex-type Fluidic Diode Port 설계 방법 개발

2016년 8월

서울대학교 대학원

에너지시스템공학부

신 세 린

Abstract

Design of SFR Vortex-type Fluidic Diode Port using Topology Optimization and Computational Fluid Dynamics Simulation

Serin Shin

Department of Energy System Engineering

The Graduate School

Seoul National University

Sodium-cooled Fast Reactor (SFR) is one of the Generation IV reactor concepts which is currently being researched and known to have many advantages over the existing Pressurized Water Reactors (PWRs). The SFR is generally categorized into three different designs depending on the system configuration; loop-type, pool-type, and hybrid loop-pool type. Among them, the hybrid loop-pool type SFR has been proposed by INL (Idaho National Laboratory) which is a combination of loop-type design is the most recent concept which is a combination of loop-type and pool-type for enhanced safety and economic feasibility. In the hybrid concept, a passive

flow control device, fluidic diode, is installed in the primary loop as a key safety component. Flow rate and thus heat removal to buffer pool are passively changed by fluidic diode according to the operation modes; normal operation or accident. Therefore the performance of fluidic diode, diodicity, is important for achieving passive safety of the system. The vortex-type fluidic diode is one of the existing passive fluidic diodes proposed for SFR applications. In order to achieve improvement of the existing design with enhanced diodicity, this study applied topology-optimization to the axial port of the vortex-type fluidic diode.

Topology optimization is a mathematical method to optimize material distribution in design domain with predefined boundary condition. Design variable that makes the objective function minimum is to be obtained. In this method, Density function is used as design variable. Density function is defined on the basis of each grid predefined and the value is between 0 (solid region) and 1 (fluid region). Adding Darcy friction force term in momentum equation, flow through fluid, solid, and intermediate region can be solved with one equation. Objective function, a substitute for diodicity, is newly derived in this study for numerical stability and better topology optimization results.

In this study, 2-D axisymmetric domain is selected for axial port design optimization. Topology optimization is conducted on various Reynolds numbers and aspect ratios within laminar flow regime. Two designs with high performance are selected as the optimum design. As these designs are optimized in laminar flow regime, preliminary performance validation is conducted in order to validate port performance up to turbulent regime. It is found that the performance is similar to or even greater than that of the preliminary design. Then, the geometry is simplified by smoothing and trimming based on geometrical sensitivity study and the whole

part is finally designed by adding supporting structures to fix the central and surrounding structures.

Port performance is evaluated in detail using 3-D CFD simulation in order to validate the final design and to analyze complicated flow and vortex precisely for further design improvement. Grid model is generated using GRIDGEN and CFD analysis is performed with ANSYS CFX. Sensitivity study is conducted in order to understand effects of turbulence model, Reynolds number, and entrance/exit length. It is found that the diodicity range is 1.7~2.3 for port A and 3.7~4.5 for port B in $1\times10^4<Re<1\times10^5$. Vortex analysis is conducted to identify effects of each vortex on pressure loss, to have insight into further design improvement, and to understand physical phenomena affecting performance and structural integrity. Friction loss coefficients for the final design are evaluated using the CFD analysis results.

Keywords

Hybrid Loop-Pool SFR (Sodium-cooled Fast Reactor), Topology Optimization, Fluidic Diode, Diodicity, Computational Fluid Dynamics

Student Number: 2013-21018

List of Contents

List of Tables

List of Figures

Chapter 1

Introduction

1.1 Background

Sodium-cooled Fast Reactor (SFR) is one of the Generation IV reactors which has been widely researched for commercialization. It is known that SFRs have enhanced safety and economic feasibility compared to existing Light Water Reactors (LWRs) in that the reactor is operated in atmospheric pressure with liquid metal coolant, sodium, and spent fuel generated from LWRs is used as fuel. The system is classified into two designs, loop type and pool type, according to system configuration. The loop type carries many advantages including compactness and easier in-service inspection and maintenance. In the pool type reactor, all of the primary components including the reactor core, primary pumps, Intermediate Heat Exchangers (IHXs), and Direct Reactor Auxiliary Cooling System (DRACS) Heat Exchangers (DHXs) are immersed in a large pool of sodium. The large thermal inertia of pool makes transients milder and a loss of coolant accident extremely unlikely.

Despite of these advantages, economic competitiveness relatively low compared to LWRs is still one of the major issues that must be solved to build commercial plants. Hybrid Loop-Pool type design has been proposed by Zhang et

al. (2008) to resolve this problem by integrating system configuration of loop type and pool type as shown in Fig 1.1. The primary system, the hot pool, is a form of closed loop composed of the reactor core, primary coolant pump, and IHX. The primary loop and DHX is immersed in the cold pool (buffer pool). The hot pool and cold pool are physically separated and thermally coupled by the Pool Reactor Auxiliary Cooling System (PRACS) Heat Exchangers (PHXs). Hybrid type reactor delivers many advantages such as larger thermal inertia, lower possibility of sodium leakage, system compactness, higher power generation efficiency, and easier in-service inspection. The detailed characteristics are listed in Table 1.1.

Flow path and flow rate of primary coolant is shown in Fig 1.2. During normal operation, the reactor core is cooled by forced convective flow of sodium coolant and the heat is transferred to IHXs to generate electricity. There is a small bypass flow upward through PHX, transferring heat to the cold pool thus resulting in a certain portion of heat loss. Flow rate through PHX should be extremely low so that it does not affect system efficiency. On the other hand, under the condition of loss of forced circulation (LOFC), reactor heat is mainly transferred through PHX to the cold pool by natural circulation. Flow rate through PHX should be high enough to remove decay heat generated in the reactor core. Fluidic diode (FD) in PRACS is the key component that controls flow rate depending on operating mode. Fluidic diode is a simple passive flow control device which is designed to provide low flow resistance in the forward direction and high flow resistance in the backward direction. The performance of fluidic diode is defined as diodicity (Di),

$$\mathrm{Di} = \frac{\Delta P_{backward}}{\Delta P_{forward}} \tag{1.1}$$

the ratio of backward to forward flow pressure drop under the same boundary

condition. Passive safety of the system can be improved with higher Di. In order to enhance passive safety of the hybrid loop-pool type system, it is essential to perform study on improving performance of fluidic diode and its following components.

1.2 Previous Studies

1.2.1 Vortex-type Fluidic Diode

As illustrated in Fig 1.3, vortex-type fluidic diode consists of a disc-shaped chamber with a cylindrical axis port and a tangential port connected to the chamber. It provides high flow resistance in the backward flow, generating an irreversible loss of kinetic energy by creating a strong vortex. Only moderate flow resistance is provided to the forward flow with no vortex generated.

CFD study on flow characteristics through vortex-type fluidic diode was performed by Kulkarni et al. (2008). It was found that which factors affect fluidic diode performance – FD geometry, size, aspect ratio, port geometry, and Reynolds number. Study on design modification to improve performance was conducted on the basis of parametric change.

Full-scale experiment with water was performed by Chikazawa et al. (2009). Two types of vortex-type fluidic diodes were proposed for 50MW SFR plant. Design change was conducted to improve performance and it was found that modified design meet requirements of both normal operation and LOFC transients.

1.2.2 Topology Optimization of Fluid Flow

Topology optimization is a mathematical approach to optimize material distribution in design domain with predefined boundary condition. It has been originally used to find the best concept design in structural engineering field. The application was broaden to fluid flow area by Borrvall and Petersson (2003). Since then, topology optimization has been used with various purpose such as optimizing the air duct design in a car [Othmer, 2006], 2-D catalytic microfluidic reactor [Okkels, 2006], and 2-D fluidic diode [Lin, 2015].

As research on topology optimization of fluid flow has been conducted only for a decade, topology optimization in turbulent regime is highly limited [Yoon, 2016]. Studies on topology optimization for fluid flow are largely conducted in low Reynolds number laminar regime as of now.

1.3 Objectives and Scope

The main objectives of this study is (1) to develop the methodology of optimizing a port design based on topology optimization and (2) to validate and evaluate the optimized port performance based on CFD simulation. The whole procedure of topology optimization is implemented and conducted using COMSOL Multiphysics code. Preliminary performance validation, geometry simplification, and part design are performed using COMSOL. In order to analyze port performance in turbulent regime precisely, 3-D CFD simulation is conducted. Sensitivity study is conducted to identify the effects of various parameters such as

turbulent model, Reynolds number, and entrance/exit length. The effects of each vortex, insight into further design modification, and physical phenomena affecting performance and structure integrity are figured out by vortex analysis. Friction loss coefficient for each flow is derived from CFD analysis. The overview of the scope is illustrated in Fig 1.4

The thesis is composed according to the outline of the study. General theory of topology optimization for fluidic diode is presented in Chapter 2. In Chapter 3, the process of designing SFR vortex-type fluidic diode port based on topology optimization is described. Performance validation and evaluation for the flow passing optimum design port using CFD analysis is covered in Chapter 5.

Table 1. 1 Characteristics of hybrid loop-pool SFR (Zhang et al., 2008)

Concept	To improve safety and economic feasibility by integration existing loop type and pool type SFRs.
System configuration	• Hot pool and cold pool are physically separated and thermally coupled by PHX. • Hot pool is the primary system with the form of closed-loop and cold pool functions as a buffer pool.
Advantages	[Safety] • Peak cladding temperature during transients decreases due to improved natural circulation. • Higher thermal inertial due to lower cold pool temperature • Primary sodium leakage and core uncovery is prevented due to the primary system is immersed in the cold pool. [Economic feasibility] • Compactness IHX • The amount of sodium that should be purified is reduced due to the separated configuration of hot and cold pool. • The efficiency can be enhanced with higher inlet and outlet temperature. [Design flexibility] • The flexibility to optimize system design is achieved with separated hot and cold pool. [In-service inspection] • In-service inspection can be conducted with removing sodium coolant in cold pool only.

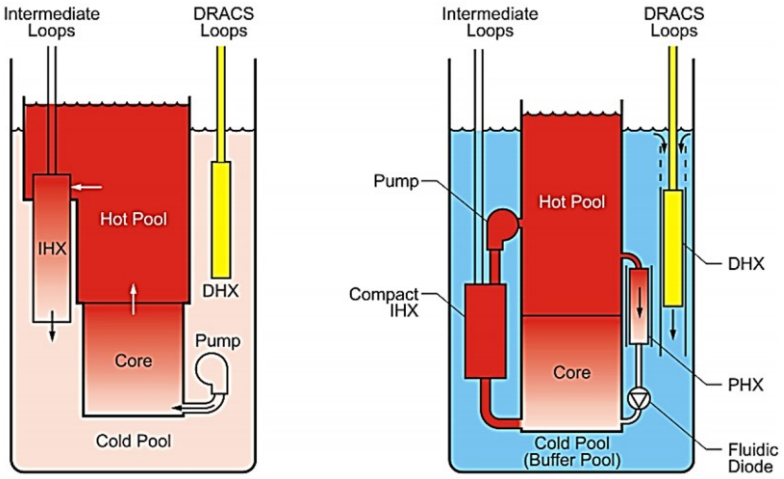

(a) Pool type (b) Hybrid loop-pool type

Figure 1. 1 SFR system configuration (Zhao et al., 2008)

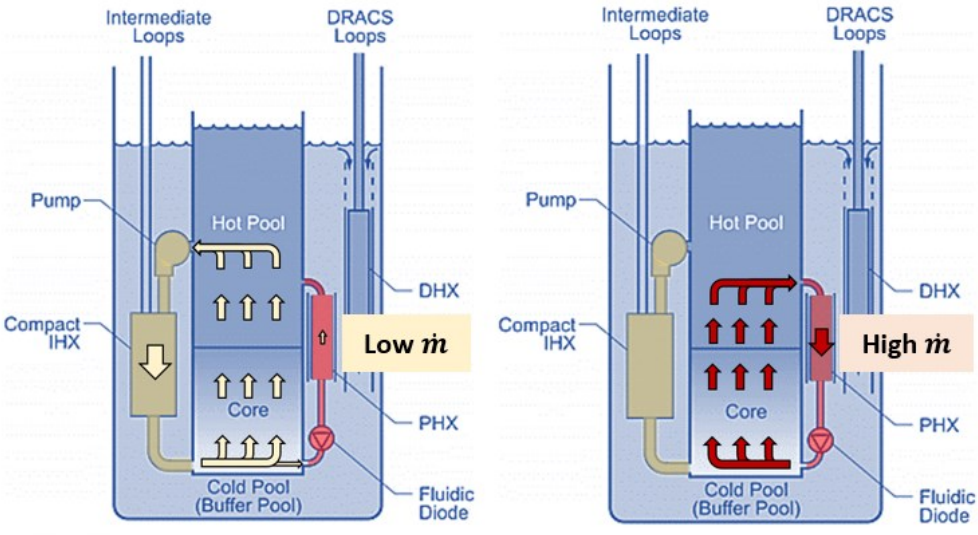

(a) Normal operation (b) LOFC

Figure 1. 2 Flow path and flow rate of primary coolant in hybrid SFR (Zhao et al., 2008)

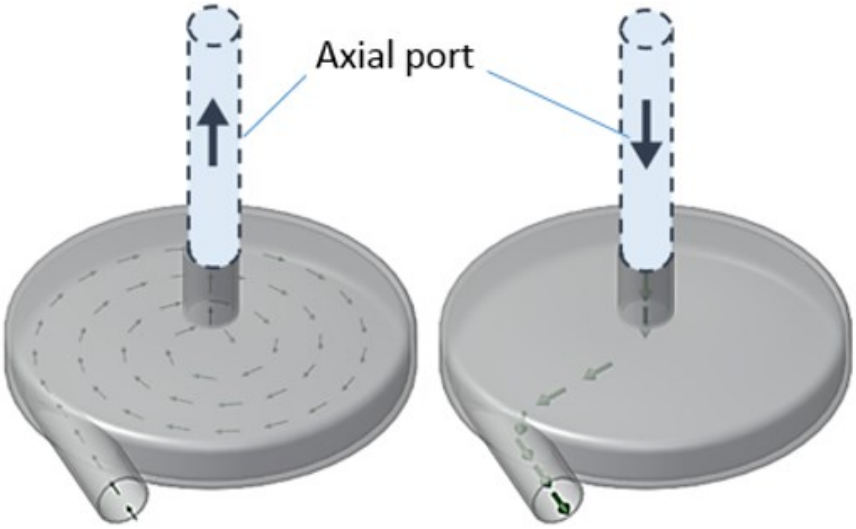

(a) Backward flow (b) Forward flow

Figure 1. 3 Vortex-type fluidic diode (Holcomb et al., 2009)

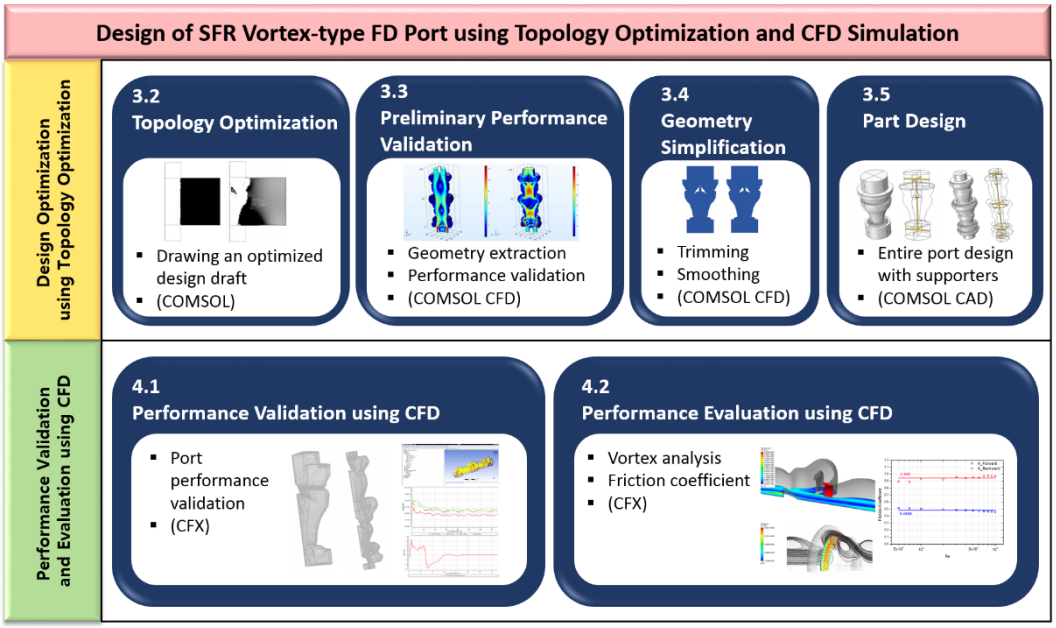

Figure 1. 4 Outline of the Study

Chapter 2

General Theory: Topology Optimization for Fluidic Diode

2.1 General Concept of Topology Optimization

Topology optimization is a mathematical method to optimize material distribution in design domain with predefined boundary condition. It has been implemented with finite element methods and numerical optimization methods such as method of moving asymptotes (MMA), genetic algorithms (GA), and sequential quadratic programming (SQP). The key virtue of this method is that it is useful for obtaining a conceptual design at the initial stage of the design process. The time and cost consumed in design process can be greatly reduced with the adoption of topology optimization in the early stage.

The fundamental concepts of fluid flow topology optimization including objective function, design variable, flow variable, constraint, and sensitivity are shown in Table 2.1. The main difference of topology optimization and conventional parametric optimization is the use of density function as design variable. As shown in Fig 2.1, density function is defined on the basis of each grid predefined and the value is ideally 0 (solid region) or 1 (fluid region). In practice, density function is

assumed to be a continuous function with the value from 0 to 1 for numerical stability and the use of gradient-based numerical optimization algorithm. Density function concept of topology optimization allows high freedom of geometry compared to other optimization method.

2.2 Basic Equations

2.2.1 Governing equation

In general hydraulic problems, mass and momentum conservation equations are solved. The equations are as follows.

$$\frac{\partial \rho}{\partial t} + \rho\left(\nabla \cdot \bar{u}\right) = 0 \tag{2.1}$$

$$\rho \frac{\partial \bar{u}}{\partial t} + \rho\left(\bar{u} \cdot \nabla\right)\bar{u} = -\nabla p + \mu \nabla^2 \bar{u} + \bar{f}_v \tag{2.2}$$

where ρ is the density, μ is the viscosity, $\bar{u}$ is the velocity field, p is the pressure field, and $\bar{f}_v$ is the external force applied to the unit volume.

Likewise, these equations are solved for topology optimization of fluid flow problems with some modification. Continuity equation for incompressible flow is the same as general one as shown below.

$$\nabla \cdot \bar{u} = 0 \tag{2.3}$$

For the momentum equation, a term that represents Darcy friction force is added to represent frictional force on fluid in intermediate region ($0 < \gamma < 1$). Darcy friction force that assumes friction proportional to velocity is given as

$$\bar{f} = -\alpha \bar{u} \tag{2.4}$$

where α is the degree of the impermeability. α is a function of density function (γ) expressed as

$$\alpha(\gamma) = \frac{\mu}{\kappa(\gamma)} = \alpha_L + (\alpha_U - \alpha_L)\frac{q(1-\gamma)}{q+\gamma} \tag{2.5}$$

α_L is the lower limit of α and usually set as zero while α_U is the upper limit of α and usually set as infinitely large value. q is a parameter to control convexity of α as shown in Fig 2.2(a).

By adding friction force term, flow through fluid, solid, and intermediate region can be solved with one momentum equation. In fluid region ($\gamma = 1$), α becomes zero resulting momentum equation the same as Navier-Stokes equation as shown below.

$$\rho\frac{\partial \bar{u}}{\partial t} + \rho(\bar{u}\cdot\nabla)\bar{u} = -\nabla P + \mu\nabla^2\bar{u} \tag{2.6}$$

In solid region ($\gamma = 0$), however, α becomes infinitely large, making flow velocity zero.

$$\bar{u} = 0 \tag{2.7}$$

In intermediate region ($0 < \gamma < 1$), α is neither zero nor infinitely large number. Therefore, the equation becomes Brinkman equation for flow passing porous media as follows.

$$\rho\frac{\partial \bar{u}}{\partial t} + \rho(\bar{u}\cdot\nabla)\bar{u} = -\nabla P + \mu\nabla^2\bar{u} - \alpha\bar{u} \tag{2.8}$$

2.2.2 Objective Function

The objective of this study is to minimize the reciprocal of diodicity. This can

be directly applied as an objective function for topology optimization but it is found that numerical instability occurs and poor topology optimization results are obtained in this case. To solve this problem, a new parameter is derived and set as an objective function for this study. It is the ratio of forward to backward flow of energy dissipation rate [Borrvall, 2003]. It is newly derived in this study from the entropy generation minimization (EGM) theory and the derivation is displayed in Appendix A. It is found that the original objective is maintained while numerical stability and better topology optimization results are obtained.

2.2.3 Penalization

There is intermediate region in topology optimization where density function is between 0 and 1. In fluid flow problems, it represents flow passing porous media with frictional force applied. In solid problems, it represents a region where two types of solid materials are mixed. For both of problems, not only either the friction force applied to flow or material properties of intermediate region need to be interpolated in terms of density function but also intermediate region should be excluded from the optimization results for manufacturability. Interpolation for this purpose is called penalization. In fluid flow problems, aforementioned Brinkman penalization is used. The friction force applied to fluid is interpolated as a function of density function. The convexity of interpolation function is determined by parameter q. For solid problems for optimizing distribution of solid material A and B, Solid Isotropic Material Penalization (SIMP) is used. The material property (ϕ) of intermediate region is a function of density function as shown below

$$\phi(\gamma) = \gamma^p \phi_A + \left(1 - \gamma^p\right)\phi_B \tag{2.9}$$

and the value is between ϕ_A and ϕ_B. The convexity of interpolation function is determined by parameter p. The function profiles depending on density function and parameter q and p are shown in Fig 2.2.

2.2.4 Constraints

Constraints are conditions that should be met by design and flow variables during the optimization process. The default conditions for topology optimization of fluid flow problems are governing equations and limit on density function. Mass and momentum conservation should be satisfied and density function value on each grid point is limited between 0 and 1. Other conditions can be applied by user depending on the objective and problem characteristics. Several constraints and their meanings are given is Table 2.2.

2.3 Optimization Algorithm

The general algorithm of topology optimization is shown in Fig 2.3. At first, design domain is selected and discretized. Initial conditions and boundary conditions of flow are applied and objective function is chosen. Initial design, density function field at the initial stage, is set and objective function is evaluated on the initial design using CFD analysis code. Sensitivity analysis is conducted using adjoint method which is efficient in case of large number of design variables. Based on the sensitivity analysis results, numerical optimization gives a modified design. And the same process as before is repeated for the modified design until the

optimization convergence criteria is met.

Table 2. 1 Fundamental concepts of fluid flow topology optimization

Concepts	**Meanings**	**Examples**
Objective function ($\Phi(\gamma, s(\gamma))$)	variables to be minimized	pressure drop, surface temperature, etc.
Design variable (γ)	variables defining the geometry	density function
Flow variable ($\mathrm{s}(\gamma)$)	flow-related variables obtained from the geometry(γ) by CFD analysis	velocity field, pressure field
Constraint ($\mathrm{R}(\gamma, s(\gamma))$)	conditions which should be satisfied by design and flow variables during optimization process	continuity eq., momentum eq., etc.
Sensitivity ($\frac{d\Phi}{d\gamma}$)	rate of change of objective function w.r.t design variables which determine accuracy and efficiency of optimization process	

Table 2. 2 Constraints of topology optimization

Constraint	**Meaning**
$\mathrm{R}(\gamma, \mathbf{s}) = 0$	Governing equations (continuity eq., and momentum eq.) should be satisfied.
$0 \leq \gamma \leq 1$	Density function value on each grid point is limited between 0 and 1.
$\sum_{i=1}^{N} \gamma_i \leq \mathrm{V}$	A total amount of material in design domain is limited below V.
$\int_{\Omega} \left[\left(\frac{\partial \gamma}{\partial r} \right)^2 + \left(\frac{\partial \gamma}{\partial z} \right)^2 \right] d\Omega \leq 200$	To avoid small pockets of intermediate region when the design domain is 2-D axisymmetric domain

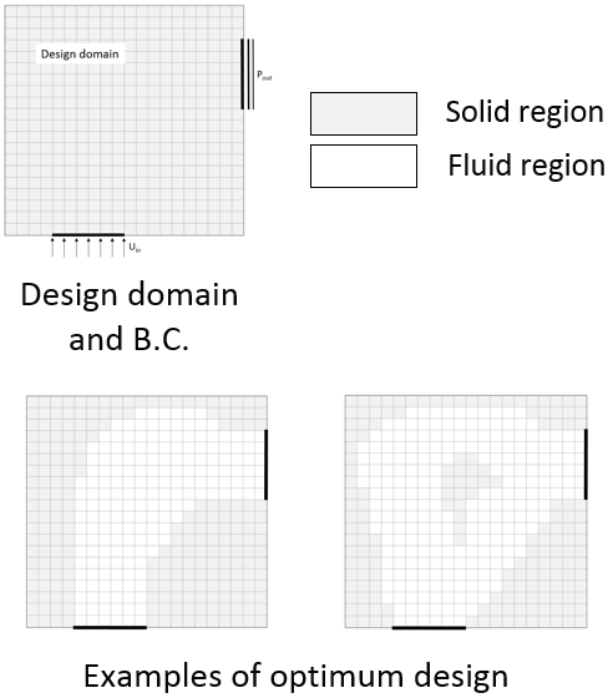

Figure 2. 1 Illustration of topology optimization based on density function

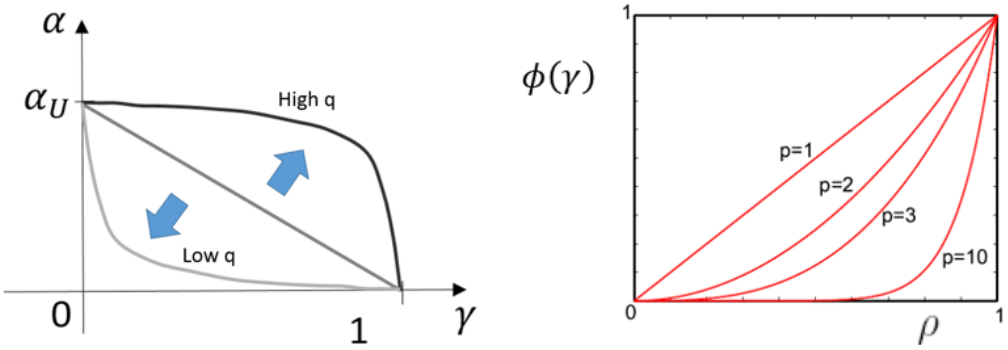

(a) Brinkman penalization (b) SIMP

Figure 2. 2 Penalization function

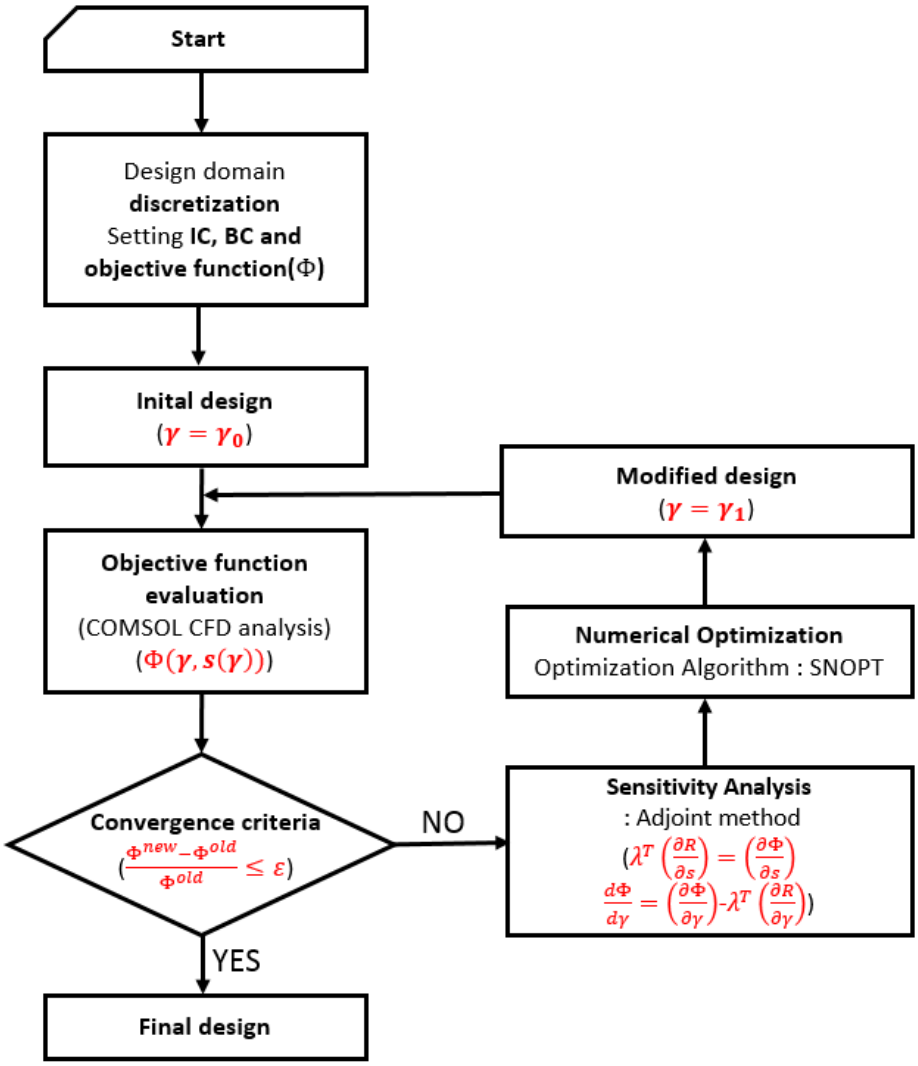

Figure 2. 3 General algorithm of topology optimization method

Chapter 3

Design of SFR Vortex-type Fluidic Diode Port using Topology Optimization

3.1 Design Methodology

The overall design methodology adopted in this study is shown in Fig 3.1. The procedure consists of two stages; (1) Design optimization using topology optimization and (2) Performance validation and evaluation using CFD.

In the first stage, an optimized design draft is drawn from topology optimization analysis using COMSOL. Since topology optimization is conducted only in low Reynolds laminar regime, performance in turbulent regime is preliminarily validated using COMSOL CFD. Geometry simplification is conducted next to remove complicated structures and ensure manufacturability. After adding supporting structures to central and surrounding structures in the port, the first stage is completed.

In the second stage, performance validation and evaluation using 3-D CFD analysis are conducted to investigate port performance thoroughly. Sensitivity study is conducted in order to identify the effect of parameters on the performance. Based on CFD analysis results, insight into further design modification is obtained and

physical phenomena affecting performance and structural integrity is identified as well as the effect of each vortex is identified.

3.2 Topology Optimization

3.2.1 Geometry and Model Domain

The objective of this study is to draw an optimized design for the axial port of vortex-type fluidic diode. As can be seen in Fig 3.2, 2-D axisymmetric domain is used with the assumption of axial port having no azimuthal dependency. Both inlet and outlet are located at a distance L_{ent} from the design domain for numerical stability of topology optimization in the vicinity of inlet and outlet. In this study, the ratio of r_{ent} and R is fixed as 1:3.5 and aspect ratio (AR) is defined as the ratio of r_{ent} and L.

3.2.2 Assumptions and Conditions

In order to obtain conceptual design for axial port, topology optimization is conducted using COMSOL. Two fundamental assumptions are made for this study; (1) the design with high diodicity in laminar regime will also provide high diodicity in turbulent regime and (2) the port design and performance will vary with respect to Reynolds number and aspect ratio. According to these assumptions, parametric study is conducted on the selected Reynolds numbers and aspect ratios as shown in Table 3.1.

As depicted in Fig 3.3, design domain is discretized with triangular unstructured grid. The detailed mesh information for each geometry is given in Table 3.2. The minimum element quality is maintained above 0.75 and average element quality above 0.98. Boundary layer grid is not applied because of the limitation of topology optimization.

For the analysis following assumptions are made; (1) steady-state, (2) incompressible flow, (3) laminar flow, (4) no heat transfer and (5) constant viscosity.

Boundary conditions are applied to inlet, outlet and wall. Fully-developed laminar flow velocity profile is assumed at inlet while zero gauge pressure is assumed at outlet. No-slip condition is applied to wall.

3.2.3 Optimization Formulation

For each parametric case, following physical models are solved in the entire domain.

Mass continuity equation

$$\nabla \cdot \bar{u} = 0 \tag{3.1}$$

Momentum conservation equation

$$\rho \frac{\partial \bar{u}}{\partial t} + \rho\left(\bar{u} \cdot \nabla\right) = -\nabla P + \mu \nabla^2 \bar{u} - \alpha \bar{u} \tag{3.2}$$

where the degree of impermeability, α, is as below

$$\alpha(\gamma) = \frac{\mu}{\kappa(\gamma)} = \alpha_L + \left(\alpha_U - \alpha_L\right)\frac{q(1-\gamma)}{q+\gamma} \tag{3.3}$$

and topology optimization parameters are selected as a constant; $\alpha_L = 0$, $\alpha_U = 1 \times 10^{10}$ and $q = 1 \times 10^{7}$.

Initial design should be well defined because topology optimization has high dependency on the initial design. A trial-and-error approach is made to find an appropriate initial design referring to the previous works. And the condition that gives the best topology optimization result is selected as an initial design for this study as shown in Fig 3.4. In the design domain, initial density function is set as unity if $r<r_{ent}$ while a constant between 0.5 and 0.7 if $r>r_{ent}$.

Objective function is set as the ratio of forward to backward flow of energy dissipation rate as shown below

$$\Phi = \frac{E_{forward}}{E_{backward}} \tag{3.4}$$

where energy dissipation rate is sum of viscous dissipation and frictional dissipation as follows.

$$E = E_{viscous} + E_{friction} \tag{3.5}$$

$$E_{viscous} = \int_{\Omega} \mu \left[2\left\{ \left(\frac{\partial u_r}{\partial r} \right)^2 + \left(\frac{u_r}{r} \right)^2 + \left(\frac{\partial u_z}{\partial z} \right)^2 \right\} + \left(\frac{\partial u_r}{\partial z} + \frac{\partial u_z}{\partial r} \right)^2 \right] d\Omega \tag{3.6}$$

$$E_{friction} = \int_{\Omega} \alpha(\gamma)\left({u_r}^2 + {u_z}^2 \right) d\Omega \tag{3.7}$$

Ω is design domain and above equation is simplified form for 2-D axisymmetric domain.

Excluding the governing equation, in total 2 constraints are applied for this study. Pointwise density function constraint ($0 \leq \gamma \leq 1$) is applied for each grid point. To avoid small pockets of intermediate region, integral inequality constraint simplified for 2-D axisymmetric domain is applied as shown below.

$$\int_{\Omega}\left[\left(\frac{\partial\gamma}{\partial r}\right)^2+\left(\frac{\partial\gamma}{\partial z}\right)^2\right]d\Omega \le 200 \tag{3.8}$$

3.2.4 Topology Optimization Results

Topology optimization is conducted on predefined parametric cases. The optimized density function distribution is displayed in Fig 3.5 and the performance and pressure drop is given in Table 3.3. Velocity field and streamline of each case is shown in Fig 3.6 to Fig 3.9.

It is found that the quality of topology optimization results of high aspect ratio cases is higher than that of low aspect ratio since there is little intermediate region and almost all grid points have density function value zero or unity. Comparing the effects of parameters, aspect ratio is found to have higher effect than Reynolds number because the optimized design has little difference with regard to Reynolds number while significant difference is observed with regard to aspect ratio. The difference between the same aspect ratio cases is explained with the existence of many local optimum points that can be reached by a little change of initial and boundary conditions. The small fluid region shown in solid region is maintained once generated as it is neglected during iteration process because it does not affect performance.

At the same aspect ratio condition, performance increases as Reynolds number increases. At the same Reynolds number condition, performance increases as aspect ratio increases partly because of the longer port length.

In this study, optimized design should be selected for following port design process. As the effect of Reynolds number is small compared to that of aspect ratio,

the designs of highest Reynolds number are chosen as candidate for optimum designs. Among the designs of highest Reynolds number, two designs of high performance and high quality of topology optimization result are selected and designated as optimum design A and B as shown in Fig 3.10.

Similarity validation is conducted to identify that the same performance is maintained on a large-scale domain with the same Reynolds number flow. The original flow equation is Eq. (3.2) and non-dimensionalized flow equation is expressed as

$$\frac{\partial \bar{u}^*}{\partial t^*} + \bar{u}^* \cdot \nabla \bar{u}^* = -\nabla P^* + \frac{1}{\mathrm{Re}} \nabla^2 \bar{u}^* - \frac{1}{\mathrm{Re}} \frac{1}{\mathrm{Da}} \bar{u}^* \tag{3.9}$$

where Darcy number, Da, is defined as follows.

$$\mathrm{Da} = \frac{\mu}{\alpha_U D^2} \tag{3.9}$$

CFD analysis is conducted on both small and large scale of optimum design A when the dimensionless numbers, Re and Da, are kept the same. The geometry dimensions are shown in Table 3.4 and dimensionless velocity and pressure results are shown in Fig 3.11 and Table 3.5, respectively. The results show that the port performance is maintained regardless of the geometry scale if dimensionless numbers, Re and Da, are kept the same.

3.3 Preliminary Performance Validation

3.3.1 Geometry Extraction from Topology Optimization

As topology optimization result is given as a continuous density function distribution between 0 and 1, clear geometry should be extracted from the result. In this study, a contour line of density function equal to 0.5 is defined as the optimum geometry as shown in Fig 3.12. Small geometries that does not affect performance are removed in advance of preliminary performance validation.

3.3.2 Performance Validation using Preliminary CFD Simulation

It is assumed that the high performance of the port design in laminar regime will be maintained in turbulent regime prior to conducting topology optimization as described in Section 3.2.2. Therefore, it needs to be validated that the assumption is valid in reality. CFD simulation is conducted on 2-D axisymmetric optimum design A and B with turbulent flow (3×10^3<Re<5×10^5). RANS k-e model with default parameters is used in COMSOL CFD. Performance with regard to Reynolds number is shown in Fig 3.13. It is found that the performance is similar to or greater than the designed value. Velocity field profile is given in Fig 3.14. In COMSOL CFD, wall function for k-e model is implemented so that y+ becomes 11.06 which corresponds to the distance from the wall where the logarithmic layer meets the viscous sublayer if the boundary mesh is sufficiently fine. Thus, y+ is checked for all cases and it is found that y+ is 11.06 at the wall for all cases as shown in Fig. 3.15.

3.4 Geometry Simplification

The design obtained from topology optimization has many small structures inside the flow channel and roughness on the surface, which is not preferable. For this reason, geometry simplification is conducted with modification that does not significantly reduces the performance.

Geometry simplification is conducted in two stages; (1) Trimming and (2) Smoothing. Small structures are expected to have little effect on port performance while they deteriorate manufacturability. Therefore it is required to remove small structures in the middle of the port channel based on the degree of influence they have on performance. Likewise, wall roughness can be smoothed once it is proved that performance is maintained. The effect of each structures are identified by sensitivity analysis.

3.4.1 Trimming

There are two small structures in optimum design A and six structures in optimum design B. The location and their designation is shown in Fig 3.16. CFD analysis is conducted on the original design, the design that each small structure is removed, and the design that all of the small structures are removed. Sensitivity study is conducted in three Reynolds numbers.

The result of sensitivity study is shown in Table 3.6. In case of design A, performance of the design with small structures removed is greater than the original one. Although the highest performance is shown in case of the design that only A-b is removed, it is desirable to remove all the small structures because there is little difference in performance and manufacturability can be greatly improved. In case of design B, performance increases when each of B-a, B-b, B-c, and B-f is removed

but decreases when B-d or B-e is removed. The performance of the design that all the small structures are removed except B-d and B-e has higher performance than the original one with greatly enhanced manufacturability.

3.4.2 Smoothing

After selectively removing the small structures, smoothing is conducted in two stages; (1) Smoothing the wall and (2) Smoothing the central structures. For both of cases, interpolation curve relative tolerance (ICRT) is used as a roughness control parameter. CFD analysis is conducted on the original design and three other smoothed designs in three Reynolds number.

The sensitivity study result of wall smoothing is shown in Table 3.7. Performance is enhanced with increased Reynolds number in all cases. With the fixed Reynolds number, performance increases as ICRT increases and then decreases for ICRT higher than 1×10^{-2}. Considering performance and manufacturability, ICRT is determined as 1×10^{-2} for optimum design A and B. The designs before and after smoothing the wall are shown in Fig 3.17.

The sensitivity study result of smoothing the central structures is displayed in Table 3.8. The designs before and after smoothing the central structures are shown in Fig 3.18. In this study, CFD analysis is conducted with fixed Reynolds number for each case. In the case of optimum design A, there is little performance change with regard to ICRT. Thus, for the manufacturability, ICRT of A-c1 is set as 1E-1. It is more complicated in the case of design B because there are three central structures. Since there is little difference between performances, pressure drop results shown in Table 3.9 should be considered instead. Pressure drop of forward

flow does not change as ICRT increases while that of backward flow does the same until it shows a sudden decrease at a certain value. ICRT of each structure is set as this value, 1×10^{-1} for B-c1, 6×10^{-2} for B-c2, and 2×10^{-2} for B-c3.

3.5 Part Design

A simplified geometry is obtained for each optimum design. 3-D port design is achieved by revolving the simplified geometry around the axis. As there are floating structures in the middle of the port, additional supporting structures are needed to obtain a final design. In order to minimize flow obstruction inside the port, axial-type supports are used for central structures and cross-type supports are used for surrounding structures and outside the port. The supports are cylinders with 1mm-diameter, except the cross supports connected to B-e which is a cylinder of 0.5mm-diameter. The whole part design is shown in Fig 3.19. As the central part of central structure is empty in design A, sensitivity study is conducted on empty center and filled center geometry to figure out the effect of axial port. It is found that the filled center design shows little performance change compared to the original one as shown in Table 3.10.

Table 3. 1 Parameter values for parametric study of topology optimization

Reynolds number	**Aspect ratio**
100	1:3
200	1:5
300	1:7
-	1:9

Table 3. 2 Grid information used for parametric study of topology optimization

Aspect ratio	**1:3**	**1:5**	**1:7**	**1:9**
Total number of elements	6732	10526	13798	17914
Minimum element quality	0.7619	0.7577	0.7612	0.7525
Average element quality	0.9886	0.989	0.9923	0.9896
Maximum element size (mm)	0.0083554	0.0088435	0.0080685	0.0081971

Table 3. 3 Topology optimization results (Di, pressure drop)

Aspect ratio	Re	100	200	300
1:3	Di	1.1526	1.2495	1.3419
	dP_f (Pa)	2.6003E4	1.9825E4	2.8248E4
	dP_b (Pa)	2.9970E4	2.4771E4	3.7905E4
1:5	Di	1.1728	1.1699	1.2278
	dP_f (Pa)	1.8150E4	6.0629E4	9.7393E4
	dP_b (Pa)	2.1286E4	7.0933E4	1.1958E5
1:7	Di	1.6492	2.1407	2.2593
	dP_f (Pa)	2.3749E3	4.8684E3	8.9416E3
	dP_b (Pa)	3.9168E3	1.0422E4	2.0202E4
1:9	Di	1.7187	1.9980	2.9759
	dP_f (Pa)	5.8681E3	4.0229E3	8.8339E3
	dP_b (Pa)	1.0086E4	8.0376E3	2.6289E4

Table 3. 4 Geometry dimensions of similarity validation

Parameter	Small scale	Large scale
Re	300	
Da	2.5E-6	
r_{ent} (mm)	0.1	10
R (mm)	0.35	35
L (mm)	0.3	30

Table 3. 5 Similarity validation results (Pressure field)

Δp^*	**Small scale (a)**	**Large scale (b)**	**Difference (%) ((a-b)/b)**
Forward flow	14.67	14.03	4.38
Backward flow	18.62	17.02	8.55

Table 3. 6 Sensitivity study results for geometry simplification (Trimming)

Optimum design A				
	Re / Design	3E3	5E3	1E4
Performance (Di)	Original	1.2675	1.402	1.5345
	Removal of a	1.3460	1.4725	1.5938
	Removal of b	1.3965	1.5169	1.6305
	Removal of a and b	1.3535	1.4702	1.5823
Optimum design B				
	Re / Design	3E3	5E3	1E4
Performance (Di)	Original	2.2397	2.5308	2.7834
	Removal of a	2.4016	2.7518	3.0349
	Removal of b	2.3876	2.7279	3.0092
	Removal of c	2.2812	2.5420	2.7716
	Removal of d	2.0827	2.3358	2.6090
	Removal of e	1.3736	1.5012	1.6308
	Removal of f	2.4302	2.8093	3.1256
	Removal of a, b, c, and f	2.5932	2.9192	3.1951

Table 3. 7 Sensitivity study results for geometry simplification (Smoothing the wall)

Optimum design A				
	Re / ICRT	3E3	5E3	1E4
Performance (Di)	2E-3	1.3535	1.4702	1.5823
	5E-3	1.4455	1.6712	1.7577
	1E-2	1.5568	1.7858	1.8681
	2E-2	1.3500	1.4014	1.7057
Optimum design B				
	Re / ICRT	3E3	5E3	1E4
Performance (Di)	2E-3	2.4238	2.7723	3.0784
	5E-3	2.5932	2.9192	3.1951
	1E-2	2.6983	3.0006	3.2636
	2E-2	1.9118	2.0464	2.1330

Table 3. 8 Sensitivity study results for geometry simplification (Smoothing the central structures)

Optimum design A (Re=1E4)							
	ICRT / Cental structure	1E-2	2E-2	4E-2	6E-2	8E-2	1E-1
Di	c1	2.0097	2.0214	1.9507	2.0233	2.0043	1.9902
Optimum design B (Re=5E3)							
	ICRT / Central structure	1E-2	2E-2	4E-2	6E-2	8E-2	1E-1
Di	c1	2.8757	2.8383	2.8508	2.8673	2.9477	2.9455
	c2	2.8366	2.8242	2.8581	2.8869	2.6948	2.7155
	c3	2.8366	2.8243	2.6145	2.8044	2.8169	2.8169

Table 3. 9 Sensitivity study results for geometry simplification (Smoothing the central structures of optimum design B)

Optimum design B (Re=5E3)							
Central structure	ICRT of central structure	1E-2	2E-2	4E-2	6E-2	8E-2	1E-1
c1	dP_f (Pa)	160.13	159.86	158.89	159.03	160.65	160.67
	dP_b (Pa)	460.48	453.74	452.97	455.98	473.54	473.27
	Di	2.8757	2.8383	2.8508	2.8673	2.9477	2.9455
c2	dP_f (Pa)	159.71	159.85	157.83	157.51	157.18	158.48
	dP_b (Pa)	453.02	451.44	451.10	454.73	423.57	430.35
	Di	2.8366	2.8242	2.8581	2.8869	2.6948	2.7155
c3	dP_f (Pa)	159.71	163.00	165.14	154.04	153.29	153.29
	dP_b (Pa)	453.02	460.36	431.75	432.00	431.79	431.79
	Di	2.8366	2.8243	2.6145	2.8044	2.8169	2.8169

Table 3. 10 Sensitivity study results for part design (empty center and filled center of optimum design A)

Optimum design A (Re=1E4)		
	Empty center	Filled center
dP_f (Pa)	1.80E3	1.78E3
dP_b (Pa)	3.59E3	3.63E3
Di	1.99	2.04

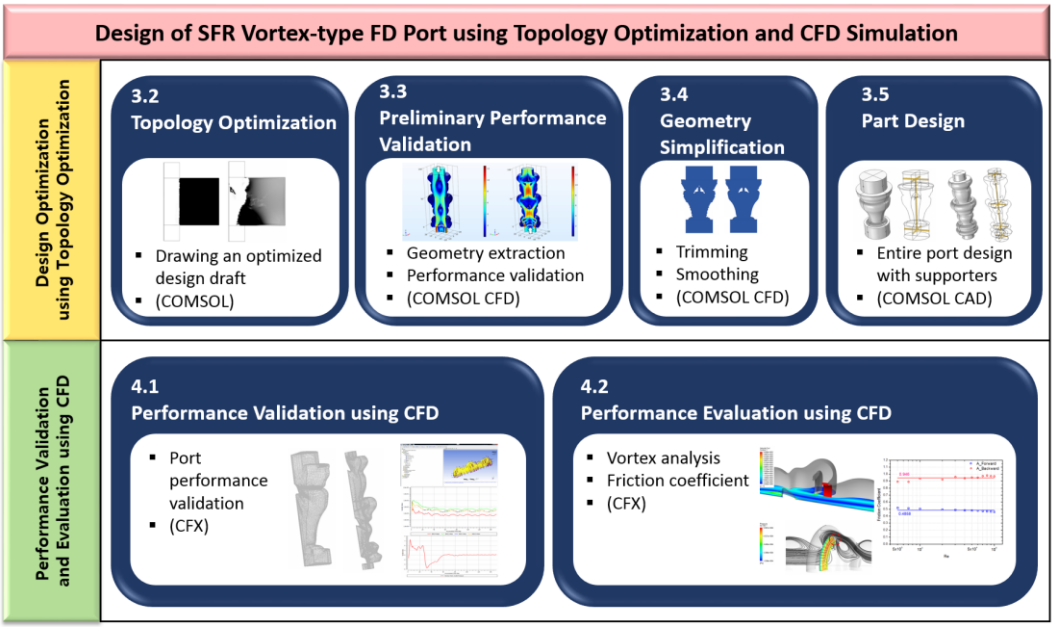

Figure 3. 1 Design methodology of the study

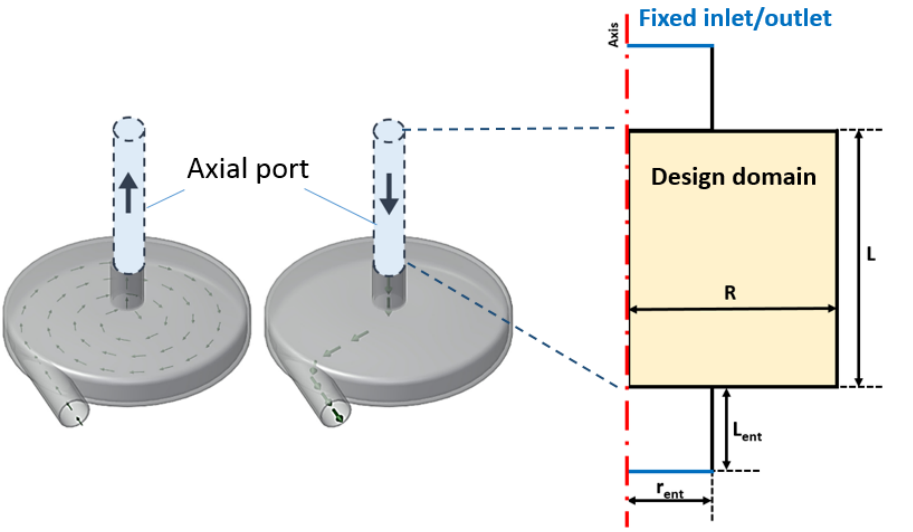

Figure 3. 2 Design domain geometry

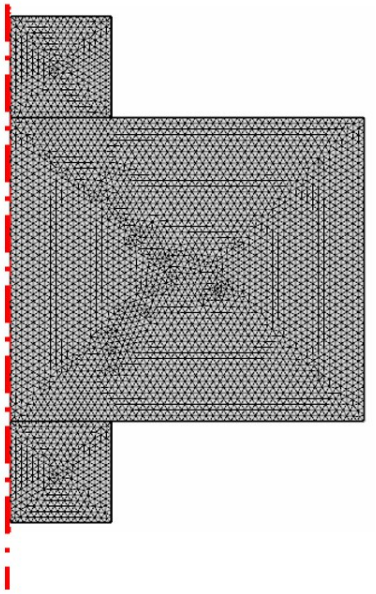

Figure 3. 3 Discretization of the entire domain of analysis (AR=1:3)

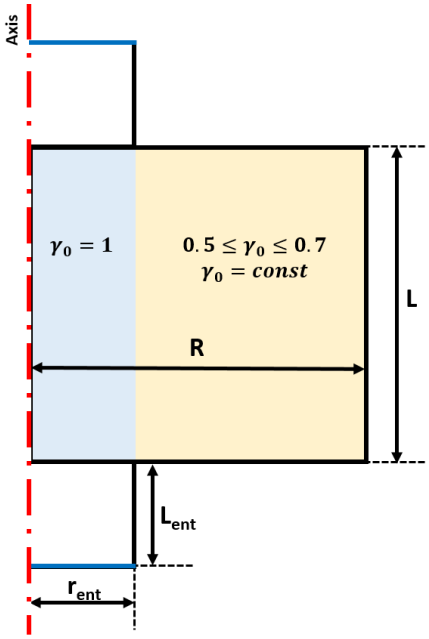

Figure 3. 4 Initial design of topology optimization

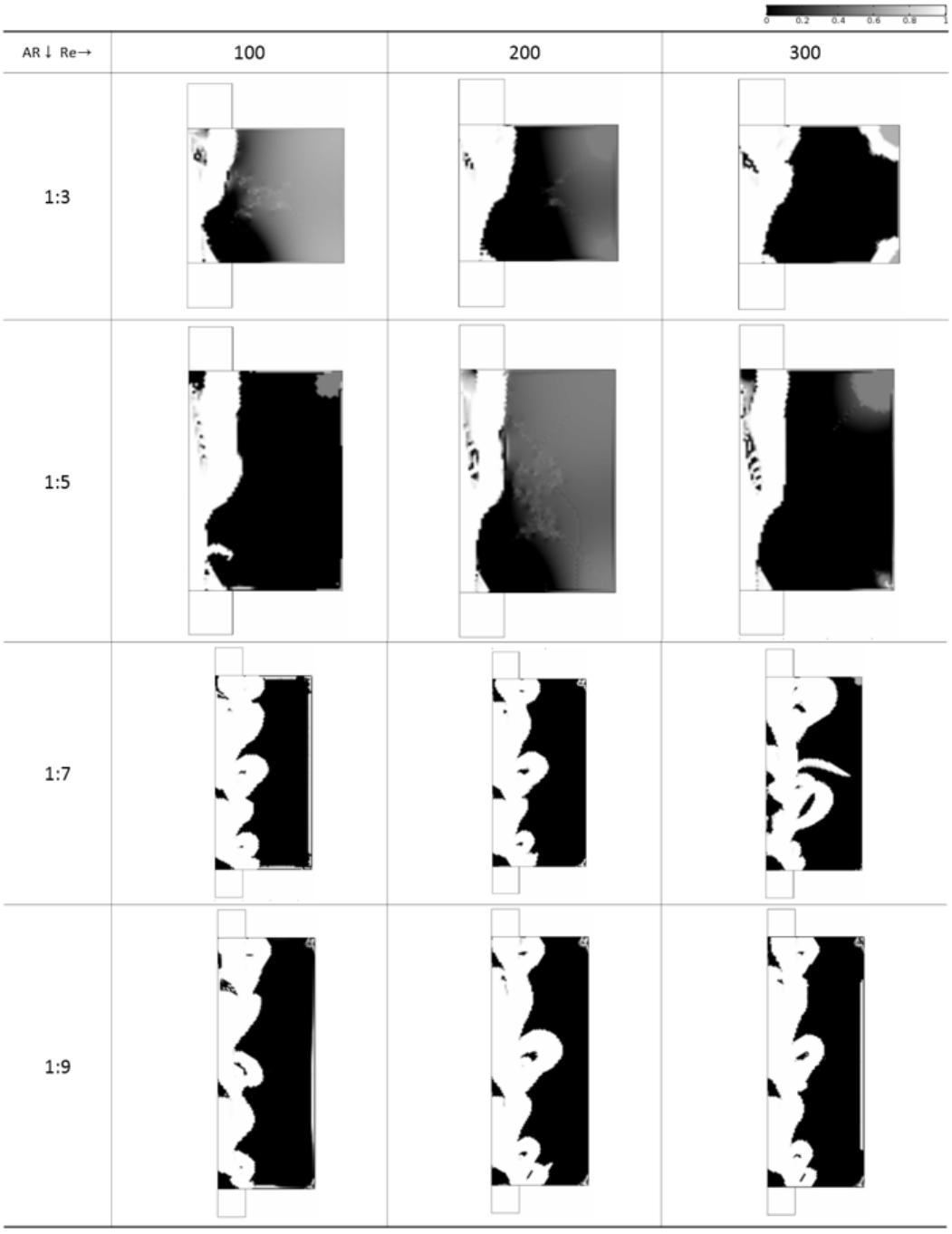

Figure 3. 5 Topology optimization results (density function)

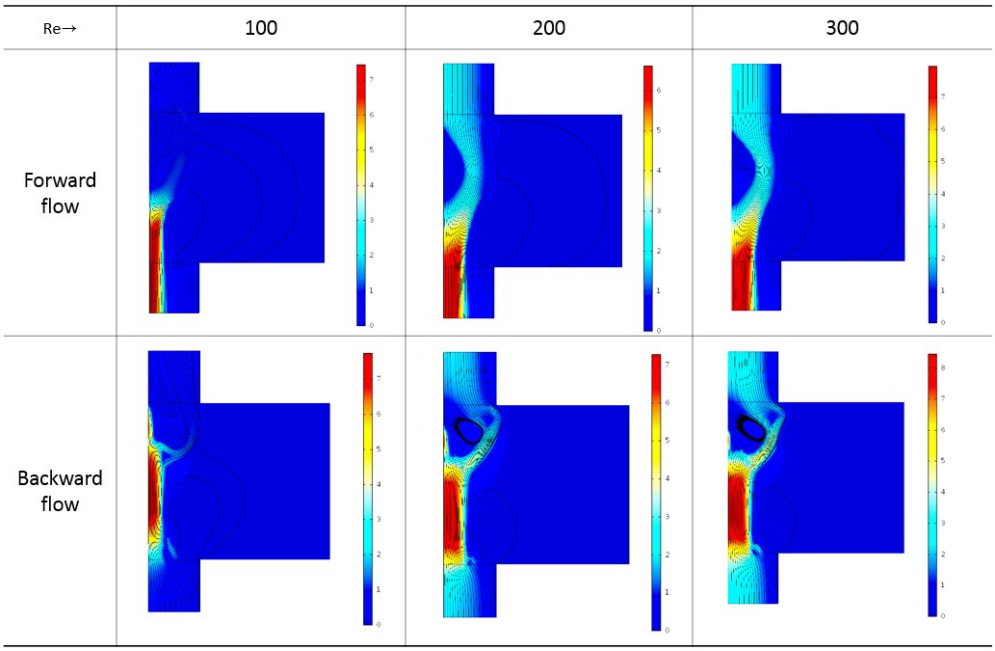

Figure 3. 6 Topology optimization results (Velocity field, AR=1:3)

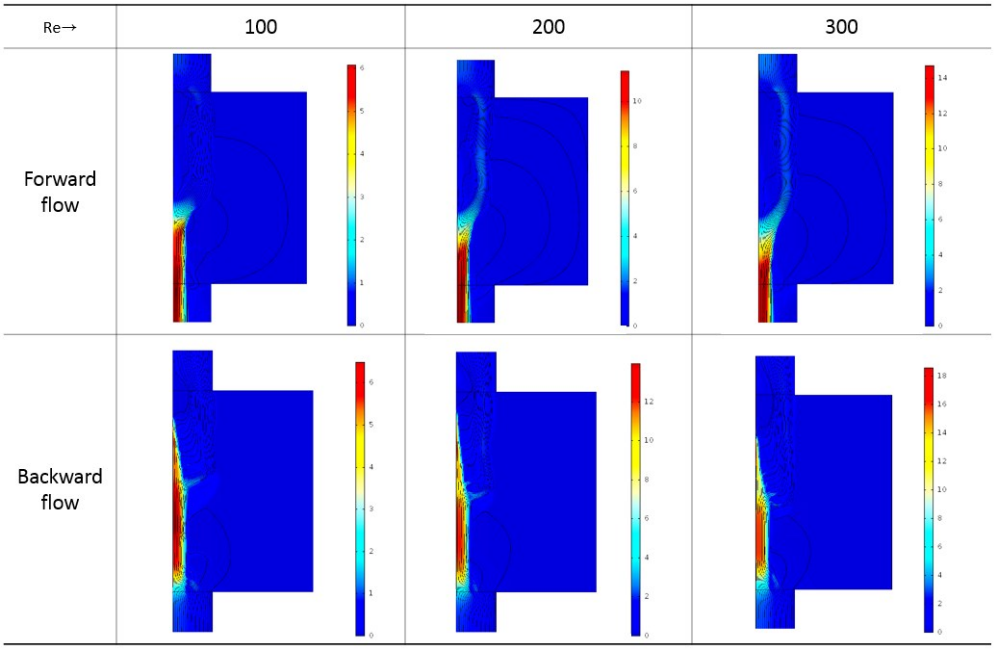

Figure 3. 7 Topology optimization results (Velocity field, AR=1:5)

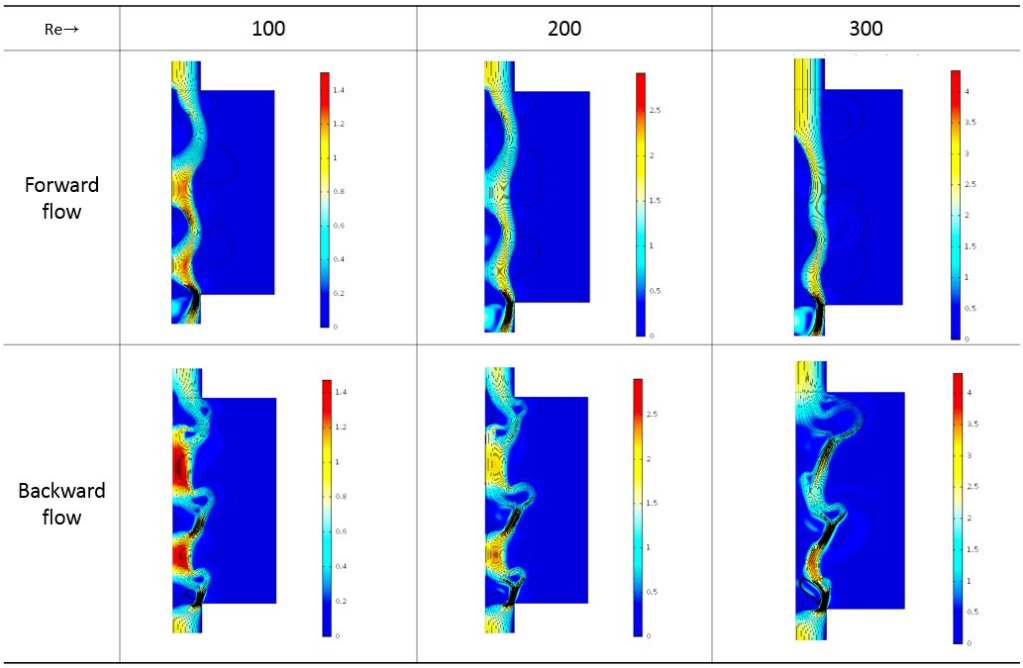

Figure 3. 8 Topology optimization results (Velocity field, AR=1:7)

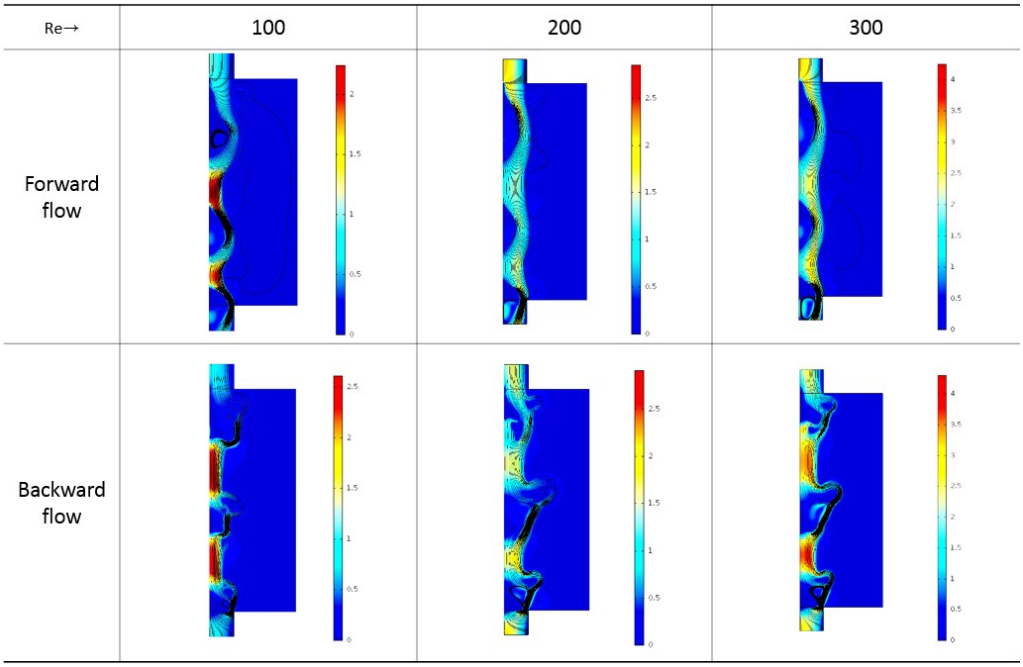

Figure 3. 9 Topology optimization results (Velocity field, AR=1:9)

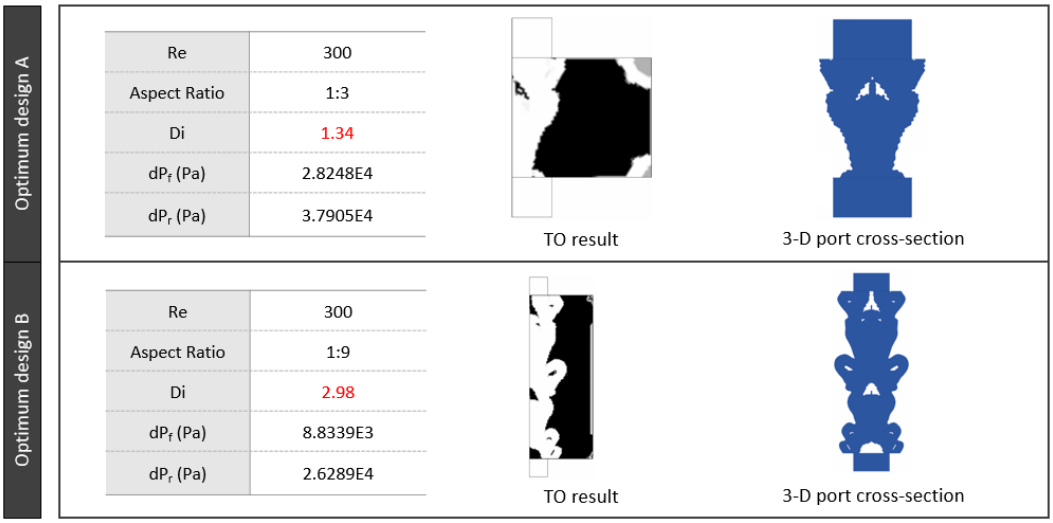

Figure 3. 10 Optimum design A and B

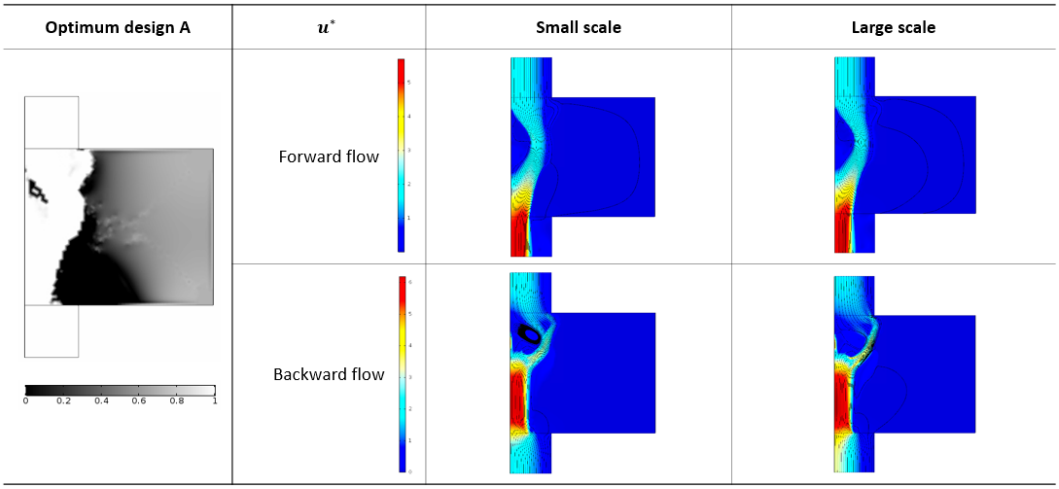

Figure 3. 11 Similarity validation result (Velocity field and streamline)

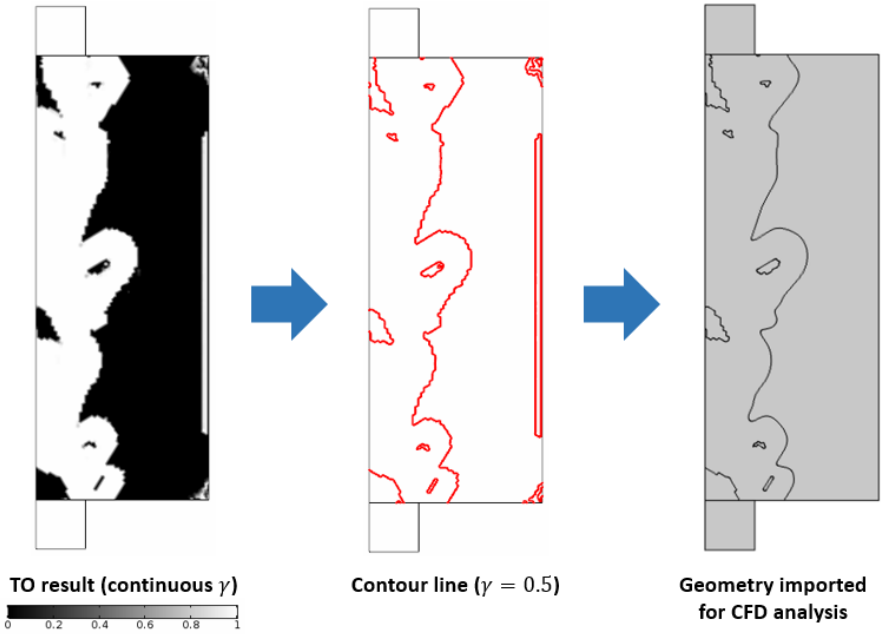

Figure 3. 12 Geometry extraction from topology optimization result

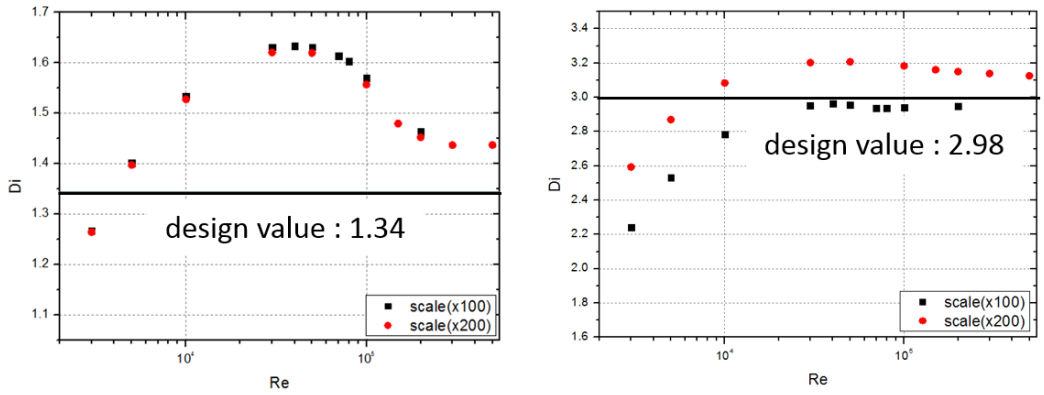

(a) Optimum design A (b) Optimum design B

Figure 3. 13 Comparison of the computed tritium concentration at the center of the wall

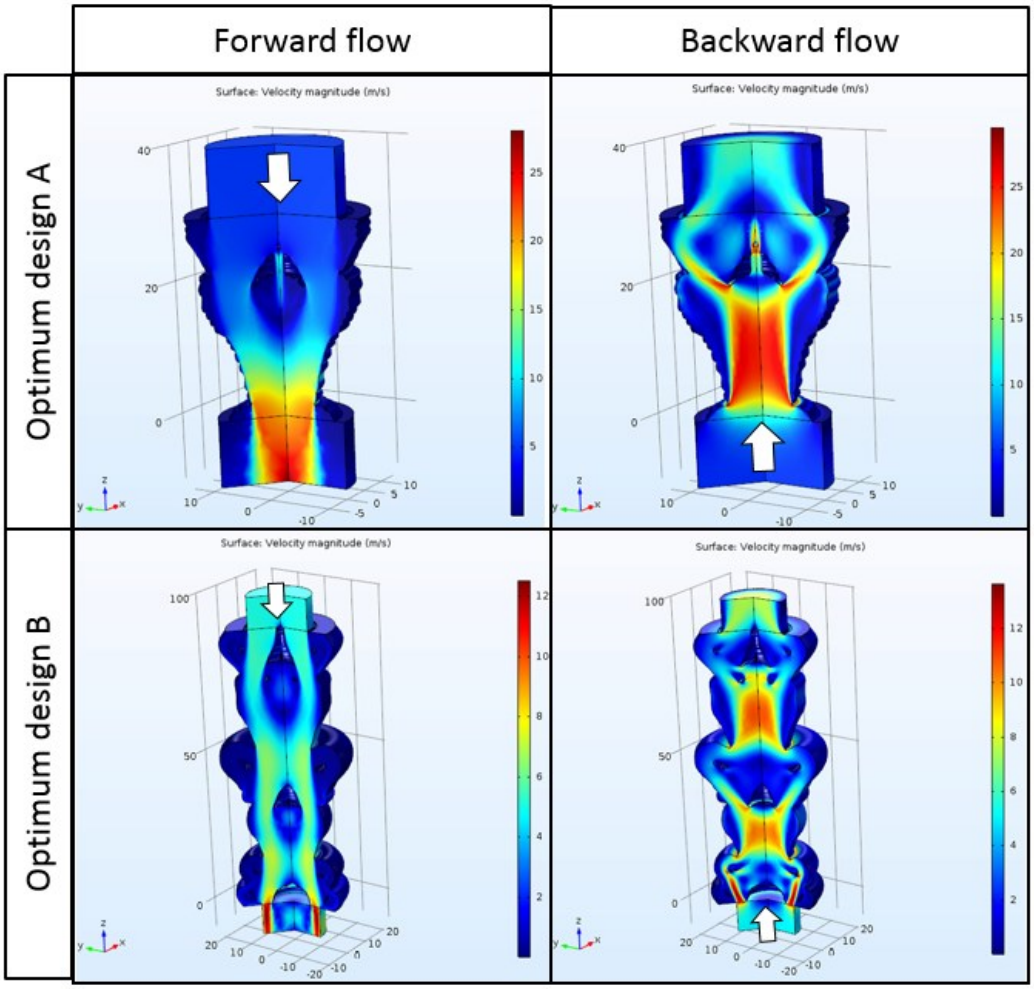

Figure 3. 14 Velocity field profile of similarity validation (Re=1E4)

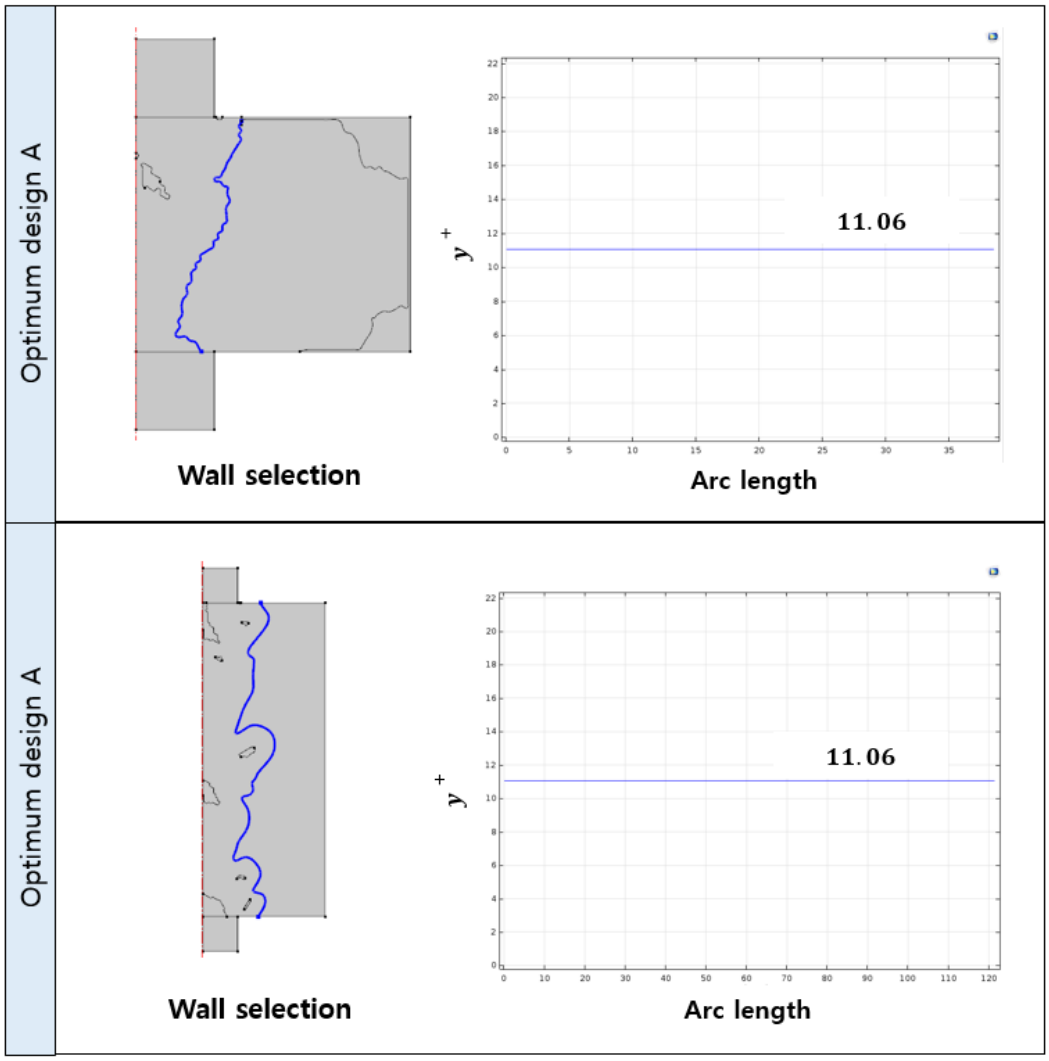

Figure 3. 15 y+ on the selected wall in COMSOL CFD

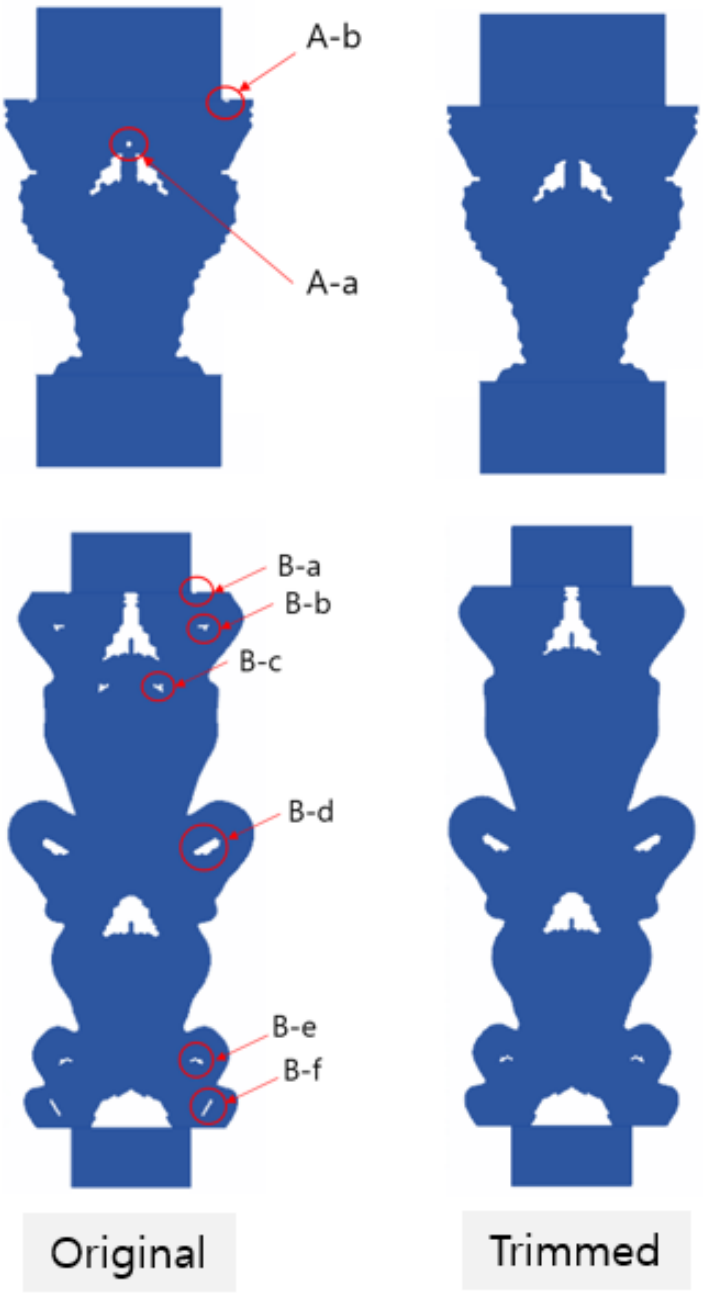

Figure 3. 16 Geometry simplification (Trimming)

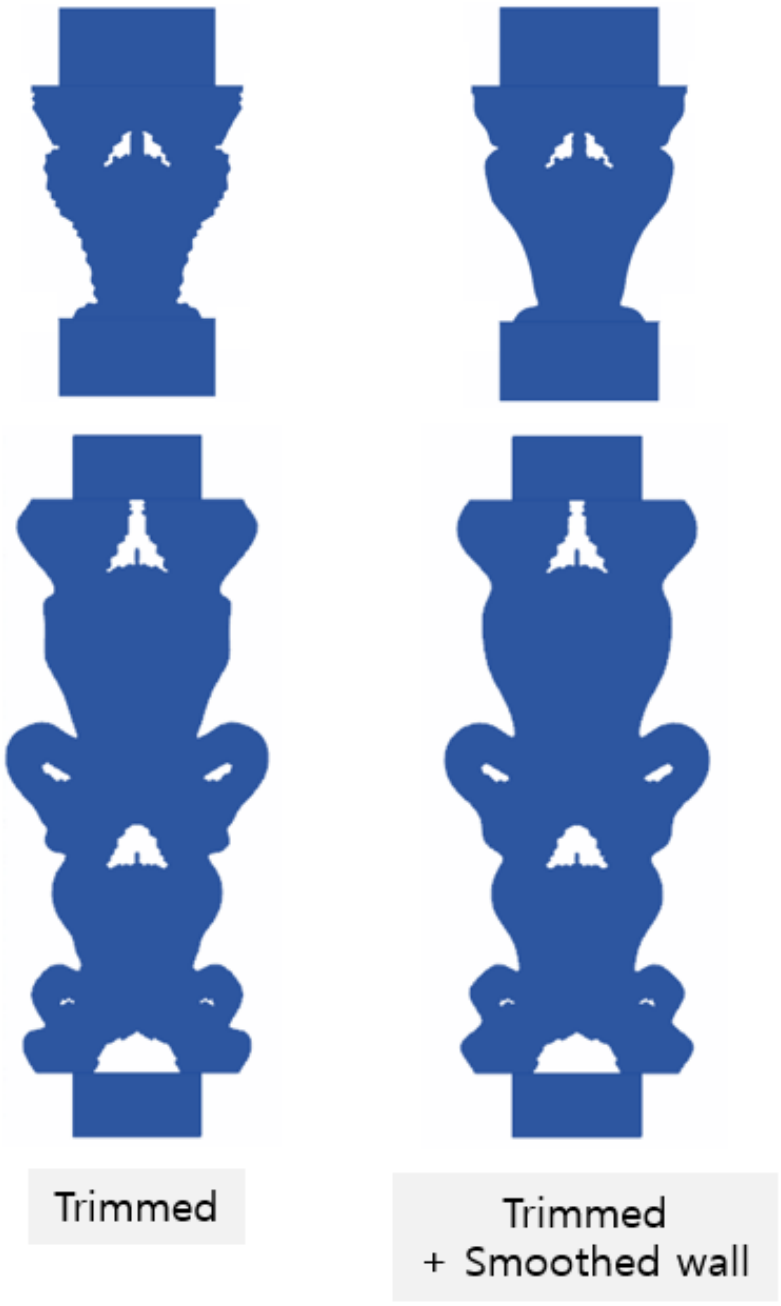

Figure 3. 17 Geometry simplification (Smoothing the wall)

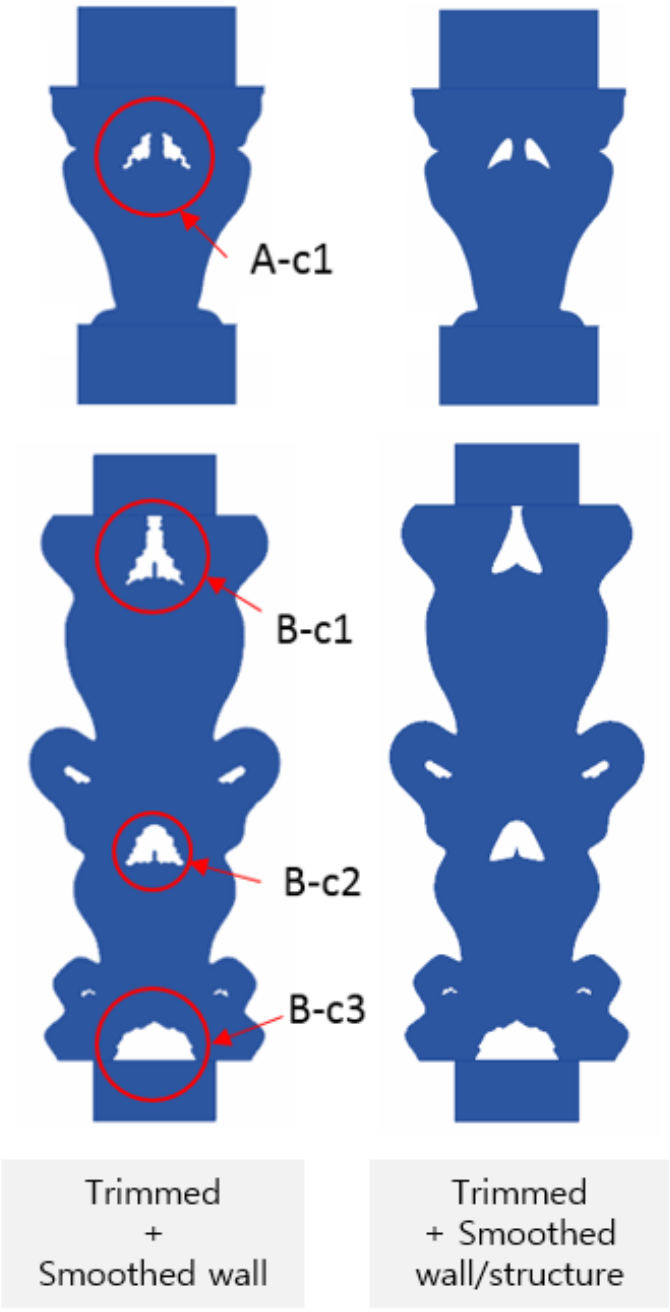

Figure 3. 18 Geometry simplification (Smoothing the central structures)

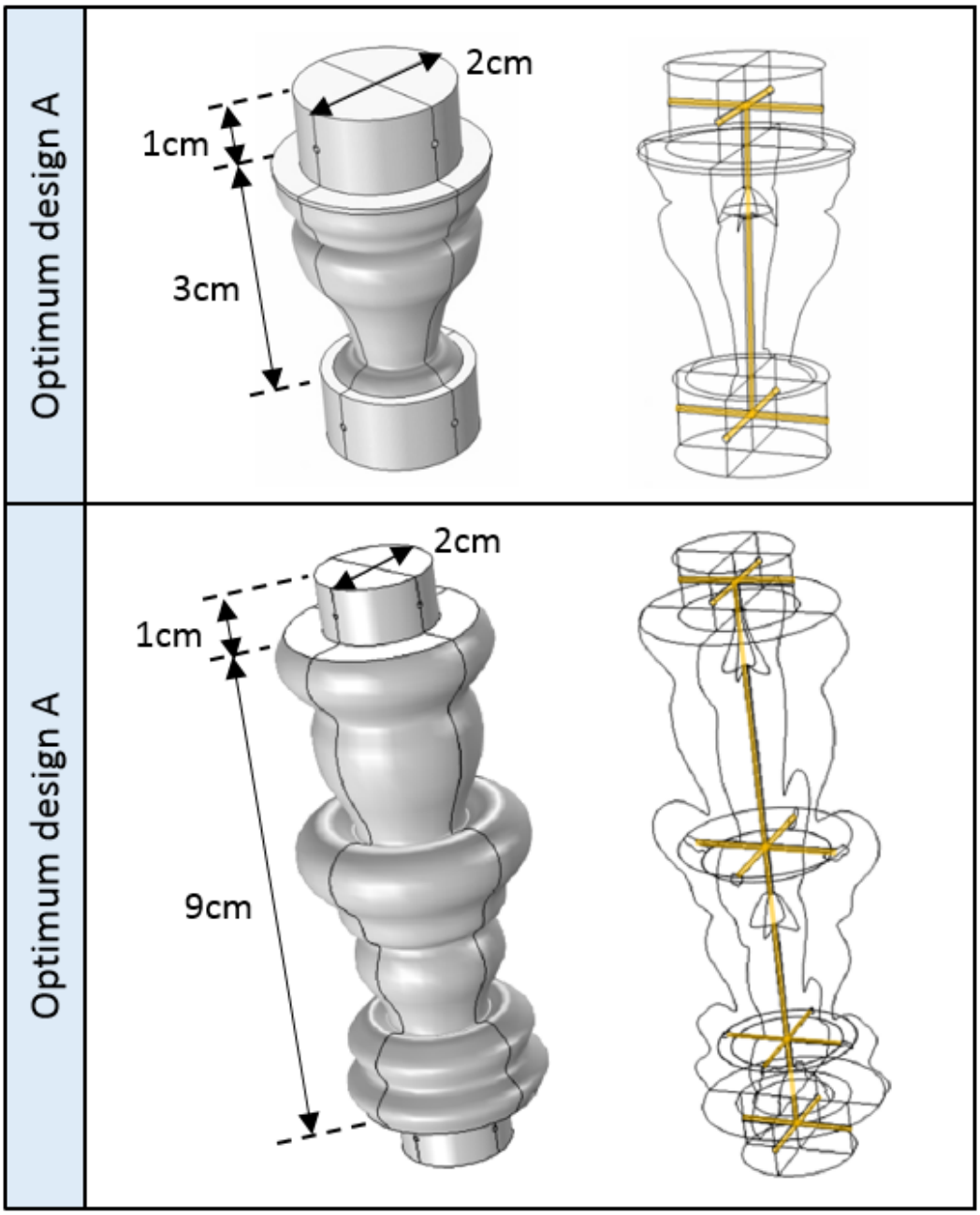

Figure 3. 19 Final part design

Chapter 4

Performance Validation and Evaluation using CFD Analysis

The performance of optimum design obtained from topology optimization was validated for both laminar and turbulent regime using simple analyses as shown in chapter 3. The result shows that performance in turbulent regime is similar to or greater than the designed value. Since the geometry has changed through geometry simplification and adding supporting structures, performance of final port design should be validated in the same way. In this case, the validation should be conducted in a more detailed manner for the following reason. There are strong vortices generated inside the port and very complicated flow due to small structures as shown in Fig 4.1. However, the COMSOL model used in preliminary validation is not quantitatively sufficient and has limitations to capture all those important phenomena. Therefore, 3-D CFD analysis using a specialized CFD software and sensitivity study is conducted on the purpose of validating performance in detail and understanding the parameters having influence on performance.

4.1 Performance Validation using 3-D CFD Simulation

4.1.1 Geometry and Mesh

3-D CFD analysis is needed to simulate flow passing port precisely. In this study, a quarter of the original 3-D domain with L_{ent}=0.5cm as seen in Fig 4.2 is set as a computational domain for accuracy and computational cost reduction.

A specialized software for high quality mesh generation, GRIDGEN, is used for grid model generation. Structured grid is generated through several iterations to catch vortex structures clearly and set y+ close to 1. The grid model is shown in Fig 4.3 and grid information is displayed in Table 4.1.

4.1.2 Assumptions and Conditions

A specialized CFD software, ANSY CFX-17.0, is used for flow field analysis. Reference pressure and temperature are 1atm and 25℃. Water is used as working fluid and no heat transfer is assumed. Turbulence model is used with the default wall function, specifically scalable wall function for k-e model and automatic wall function for k-w and SST model.

As for the wall boundary condition, no-slip condition with smooth wall option is used. Normal speed is given as the inlet boundary condition. For the outlet, boundary type is set as opening with static pressure and direction option. Relative pressure is 0 Pa and normal to boundary condition is assumed as flow direction. Rotational periodicity condition is applied with the axis parallel to flow direction as illustrated in Fig 4.4.

Advection scheme and turbulence numerics are set as high resolution. Residual type and target are set as RMS and 1×10^6, respectively.

4.1.3 Sensitivity Study

In order to identify parameters that affect performance, sensitivity study is conducted. Parameters considered in this study include turbulence model, Reynolds number, and entrance/exit length. For turbulence model, RANS-based models such as k-e, k-w, and SST are considered. Three Reynolds number in a practical range is covered. Because the optimum design A and B have flow blocking structure in the vicinity of inlet and outlet, a certain section in front of the inlet and at the back of the outlet needs to be analyzed. Thus, 0D and 10D of entrance/exit length are considered. 0D and 10D indicates the design with L_{ent} equal to 0.5cm and 20.5cm, respectively.

4.1.4 Results

A. Port Performance and Validation

3-D simulation results of entrance/exit length 0D, SST model, Reynolds number 1×10^5 are shown in Fig 4.5 and Fig 4.6. As seen in the streamline field plot, complicated flow field with strong vortices is observed due to small structures inside the port design. In both forward and backward flow, a large vortex lies on the outlet resulting much larger pressure drop than that of reality. Thus, a longer entrance/exit length is required for precise analysis. Port performance and pressure drop data is summarized in Table 4.2. It is found that y+ value range is below 14

which is appropriate for all of the turbulence models used. Diodicity is evaluated as 1.90 for optimum design A and 4.35 for design B. These are much higher than the optimized design values (1.35 for A, 1.98 for B) in laminar regime and preliminary performance validation results (1.57 for A, 2.95 for B) at the same Reynolds number using COMSOL CFD.

Since the port geometry is unique and has not been used in engineering field, it is important to validate the accuracy of CFD results by comparing with experimental data. A large vortex lying on the port outlet due to sudden expansion of flow area is similar to a vortex generated in backward-facing step (BFS) flow. Thus, the reattachment length shown in BFS flow can be a parameter to determine the accuracy of CFD simulation. The validation is conducted and identified as seen in Appendix B.

B. Performance Sensitivity

Fig 4.7 and Fig 4.8 show sensitivity study results of 3-D CFD analysis conducted on optimum design A and B, respectively. In both designs, there is no consistent tendency with regard to Reynolds number. Increase and decrease of performance are observed as Reynolds number increases. The performance estimated in 10D is greater than that estimated in 0D due to the larger pressure drop caused by a large vortex that lies on the outlet surface. The performance varies according to turbulent model used. The result of SST model is more like that of k-w model rather than k-e model. The result of k-e model shows somewhat larger difference from the others. On a basis of 10D data, the performance range is 1.7 ~ 2.3 for design A and 3.7 ~ 4.5 for design B in the region of 1×10^4<Re<1×10^4 which is greatly improved than the original design value.

4.2 Performance Evaluation using CFD Analysis

4.2.1 Vortex Analysis

Vortex analysis is a method to analyze behaviors, effects, and characteristics of vortices and widely used in mechanical engineering and aerodynamics. In this study, basic vortex analysis is conducted based on 3-D CFD analysis results for the purpose of (1) identifying effects of each vortex, (2) having insight into performance improvement by further design modification, and (3) understanding physical phenomena affecting performance and structure integrity. In this study, vortex analysis is conducted on design A and B of Re=1×10^5, SST model, entrance/exit length=10D.

Planes are located on both sides of vortices as shown in Fig 4.9 and vortices are designated as seen in Fig 4.10. And vortex type can be identified by analyzing vorticity plot as displayed in Fig 4.11. In this case, two types of vortex are observed; wake vortex and corner vortex. Wake vortex are identified with high voriticy on end point getting dispersed while corner vortex is observed in front of blocking structure as vortex filaments are accumulated. Each type of vortices is shown in Table 4.3. As for the effects of each vortex, the pressure drop and fraction of each section is identified as seen in Table 4.4. The fraction of vortex F5 is 97% which is not intended in topology optimization stage. This is due to the sudden expansion of flow channel at the outlet and can be removed with design modification resulting enhanced performance. The effect of each vortex on pressure drop for the rest of

cases are displayed in Table 4.5, Table 4.6, Table 4.7, Table 4.8, Table 4.9, and Table 4.10. Coanda effect is observed as seen in Fig 4.12. As flow follows the curved surface of central structure and vortex behind, pressure drop in this section remains low with the fraction of 1.6. Flow blockage and thus flow acceleration is observed in the outlet due to a large vortex generated as shown in Fig 4.13.

Vortex analysis on design B is conducted in the same manner. Plane location and vortex designation are shown in Fig 4.14 and Fig 4.15, respectively. Based on the vorticity plot as displayed in Fig 4.16, each type of vortex is identified as can be seen in Table 4.11. In this case, cavity vortex is observed as well as wake and corner vortex. Cavity vortex is identified with boundary layer development on end points as seen in Fig 4.17. The periodic behavior of cavity vortex can affect structural integrity and thus should be identified in further study. The effect of each vortex on pressure drop is shown in Table 4.12. As of the case of design A, pressure drop generated by a large vortex (F12) on the outlet is found to be high with the fraction of 32.3. This phenomenon, as well, is not intended and can be removed with further design modification. Flow blockage and flow acceleration is also observed in the outlet as displayed in Fig 4.18. 7 structure resulting high pressure drop. Flow attachment region is shown as high pressure region on the structure. The effect of each vortex on pressure drop for the rest of cases are displayed in Table 4.13, Table 4.14, Table 4.15, Table 4.16, Table 4.17, and Table 4.18.

4.2.2 Evaluation of Friction Loss Coefficient

Friction loss coefficient is a dimensionless parameter that represents the relation between pressure drop and flow characteristics as shown below.

$$\Delta P = f \cdot \frac{1}{2} \rho v^2 \cdot \frac{L}{D}$$

As pressure drop is important parameter for fluidic diode port design A and B, it is worth deriving friction loss coefficient. In this study, CFD analysis results of SST model and entrance/exit length 10D are used. Friction coefficient with regard to Reynolds number is shown in Fig 4.20 and Fig 4.21. Since the variation depending on Reynolds number is negligible, friction coefficient is derived as a constant for each flow by calculating an arithmetic mean of 12 cases within 5×10^3<Re<1×10^5. The derived friction coefficients are shown below.

$$f_A = \begin{cases} 0.4858 \text{ (forward flow)} \\ 0.9460 \text{ (backward flow)} \end{cases}$$

$$f_B = \begin{cases} 0.1301 \text{ (forward flow)} \\ 0.5467 \text{ (backward flow)} \end{cases}$$

Table 4. 1 Grid information

Optimum design		A	B
Number of meshes	Total	229200	543600
	Axial	191	324
	Radial	40	70
	Tangential	30	30
Boundary layer thickness (mm)			0.5

Table 4. 2 Port performance analyzed in 3-D CFD (Re=1E5, SST model, entrance/exit length=0D)

Optimum design	A	B
$y+_{forward}$	0.73-3.85	0.32-8.51
$y+_{backward}$	0.70-7.29	1.18-13.90
dP_f (Pa)	1.282E5	3.89E4
dP_b (Pa)	2.432E5	1.69E5
Di	1.90	4.35

Table 4. 3 Type of vortex (Optimum design A, Re=1E5, SST model, entrance/exit length=10D)

Forward flow		Backward flow	
Vortex	Type	Vortex	Type
F1	wake	B1	wake
F2	corner	B2	corner
F3	wake	B3	wake
F4	wake	B4	wake
F5	wake	-	-

Table 4. 4 Effects of each vortex on pressure drop (Optimum design A, Re=1E5, SST model, entrance/exit length=10D)

Optimum design A							
Turbulence model		**Forward flow**			**Backward flow**		
SST	**Total dP (Pa)**	1.007E5			2.115E5		
	Sectionwise dP (Pa)	Vortex	dP (Pa)	fraction (%)	Vortex	dP (Pa)	fraction (%)
		F1,F2	6.000E2	0.6	B1,B2	1.47E5	69.3
		F3,F4	1.600E3	1.6	B3	1.54E4	7.3
		F5	9.779E4	97.1	B4	4.38E4	20.7
	Di	2.10					

Table 4. 5 Effects of each vortex on pressure drop (Optimum design A, Re=1E4, entrance/exit length=0D)

Optimum design A							
Turbulence model		**Forward flow**			**Backward flow**		
k-e	**Total dP (Pa)**	8.068E2			1.354E3		
	Sectionwise dP (Pa)	Vortex	dP (Pa)	fraction (%)	Vortex	dP (Pa)	fraction (%)
		F1,F2	1.500E1	1.9	B1,B2	1.003E3	74.1
		F3,F4	2.400E1	3.0	B3	9.590E1	7.1
		F5	7.418E2	91.9	B4	1.351E2	10.0
	Di	1.68					
k-w	**Total dP (Pa)**	1.360E3			2.358E3		
	Sectionwise dP (Pa)	Vortex	dP (Pa)	fraction (%)	Vortex	dP (Pa)	fraction (%)
		F1,F2	1.000E1	0.7	B1,B2	1.598E3	67.8
		F3,F4	1.900E1	1.4	B3	1.779E2	7.5
		F5	1.256E3	92.4	B4	4.636E2	19.7
	Di	1.73					
SST	**Total dP (Pa)**	1.363E3			2.324E3		
	Sectionwise dP (Pa)	Vortex	dP (Pa)	fraction (%)	Vortex	dP (Pa)	fraction (%)
		F1,F2	9.000E0	0.7	B1,B2	1.671E3	71.9
		F3,F4	1.900E1	1.4	B3	1.166E2	5.0
		F5	1.259E3	92.4	B4	4.223E2	18.2
	Di	1.71					

Table 4. 6 Effects of each vortex on pressure drop (Optimum design A, Re=1E4, entrance/exit length=10D)

Optimum design A							
Turbulence model		**Forward flow**			**Backward flow**		
k-e	**Total dP (Pa)**	6.633E2			1.318E3		
	Sectionwise dP (Pa)	Vortex	dP (Pa)	fraction (%)	Vortex	dP (Pa)	fraction (%)
		F1,F2	1.180E1	1.8	B1,B2	9.475E2	71.9
		F3,F4	2.140E1	3.2	B3	1.052E2	8.0
		F5	5.560E2	83.8	B4	8.580E1	6.5
	Di	1.99					
k-w	**Total dP (Pa)**	1.110E3			2.090E3		
	Sectionwise dP (Pa)	Vortex	dP (Pa)	fraction (%)	Vortex	dP (Pa)	fraction (%)
		F1,F2	6.000E0	0.5	B1,B2	1.466E3	70.1
		F3,F4	1.700E1	1.5	B3	1.666E2	8.0
		F5	1.015E3	91.4	B4	3.023E2	14.5
	Di	1.88					
SST	**Total dP (Pa)**	1.105E3			2.045E3		
	Sectionwise dP (Pa)	Vortex	dP (Pa)	fraction (%)	Vortex	dP (Pa)	fraction (%)
		F1,F2	5.000E0	0.5	B1,B2	1.436E3	70.2
		F3,F4	1.600E1	1.4	B3	1.492E2	7.3
		F5	1.001E3	90.6	B4	3.289E2	16.1
	Di	1.85					

Table 4. 7 Effects of each vortex on pressure drop (Optimum design A, Re=5E4, entrance/exit length=0D)

Optimum design A							
Turbulence model		**Forward flow**			**Backward flow**		
k-e	**Total dP (Pa)**	1.608E4			3.073E4		
	Sectionwise dP (Pa)	Vortex	dP (Pa)	fraction (%)	Vortex	dP (Pa)	fraction (%)
		F1,F2	3.000E2	1.9	B1,B2	2.311E4	75.2
		F3,F4	5.100E2	3.2	B3	2.578E3	8.4
		F5	1.482E4	92.2	B4	2.833E3	9.2
	Di	1.91					
k-w	**Total dP (Pa)**	3.299E4			6.182E4		
	Sectionwise dP (Pa)	Vortex	dP (Pa)	fraction (%)	Vortex	dP (Pa)	fraction (%)
		F1,F2	2.300E2	0.7	B1,B2	3.985E4	64.5
		F3,F4	4.900E2	1.5	B3	4.810E3	7.8
		F5	3.116E4	94.5	B4	1.487E4	24.1
	Di	1.87					
SST	**Total dP (Pa)**	3.312E4			5.933E4		
	Sectionwise dP (Pa)	Vortex	dP (Pa)	fraction (%)	Vortex	dP (Pa)	fraction (%)
		F1,F2	2.200E2	0.7	B1,B2	4.004E4	67.5
		F3,F4	4.800E2	1.4	B3	3.430E3	5.8
		F5	3.132E4	94.6	B4	1.362E4	23.0
	Di	1.79					

Table 4. 8 Effects of each vortex on pressure drop (Optimum design A, Re=5E4, entrance/exit length=10D)

Optimum design A							
Turbulence model		**Forward flow**			**Backward flow**		
k-e	**Total dP (Pa)**	1.291E4			2.991E4		
	Sectionwise dP (Pa)	Vortex	dP (Pa)	fraction (%)	Vortex	dP (Pa)	fraction (%)
		F1,F2	2.300E2	1.8	B1,B2	2.192E4	73.3
		F3,F4	4.600E2	3.6	B3	2.700E3	9.0
		F5	1.103E4	85.4	B4	1.574E3	5.3
	Di	2.32					
k-w	**Total dP (Pa)**	2.633E4			5.416E4		
	Sectionwise dP (Pa)	Vortex	dP (Pa)	fraction (%)	Vortex	dP (Pa)	fraction (%)
		F1,F2	1.700E2	0.6	B1,B2	3.769E4	69.6
		F3,F4	4.500E2	1.7	B3	4.580E3	8.5
		F5	2.521E4	95.7	B4	9.257E3	17.1
	Di	2.06					
SST	**Total dP (Pa)**	2.622E4			5.202E4		
	Sectionwise dP (Pa)	Vortex	dP (Pa)	fraction (%)	Vortex	dP (Pa)	fraction (%)
		F1,F2	1.500E2	0.6	B1,B2	3.658E4	70.3
		F3,F4	4.100E2	1.6	B3	3.560E3	6.8
		F5	2.507E4	95.6	B4	9.936E3	19.1
	Di	1.98					

Table 4. 9 Effects of each vortex on pressure drop (Optimum design A, Re=1E5, entrance/exit length=0D)

Optimum design A							
Turbulence model		**Forward flow**			**Backward flow**		
k-e	**Total dP (Pa)**	6.875E4			1.291E5		
	Sectionwise dP (Pa)	Vortex	dP (Pa)	fraction (%)	Vortex	dP (Pa)	fraction (%)
		F1,F2	1.180E3	1.7	B1,B2	9.559E4	74.1
		F3,F4	2.010E3	2.9	B3	1.023E4	7.9
		F5	6.386E4	92.9	B4	1.534E4	11.9
	Di	1.88					
k-w	**Total dP (Pa)**	1.276E5			2.473E5		
	Sectionwise dP (Pa)	Vortex	dP (Pa)	fraction (%)	Vortex	dP (Pa)	fraction (%)
		F1,F2	9.000E2	0.7	B1,B2	1.566E5	63.3
		F3,F4	2.000E3	1.6	B3	1.874E4	7.6
		F5	1.213E5	95.1	B4	6.373E4	25.8
	Di	1.94					
SST	**Total dP (Pa)**	1.282E5			2.432E5		
	Sectionwise dP (Pa)	Vortex	dP (Pa)	fraction (%)	Vortex	dP (Pa)	fraction (%)
		F1,F2	9.000E2	0.7	B1,B2	1.585E5	65.2
		F3,F4	1.900E3	1.5	B3	1.568E4	6.4
		F5	1.221E5	95.2	B4	6.098E4	25.1
	Di	1.90					

Table 4. 10 Effects of each vortex on pressure drop (Optimum design A, Re=1E5, entrance/exit length=10D)

Optimum design A							
Turbulence model		**Forward flow**			**Backward flow**		
k-e	**Total dP (Pa)**	5.323E4			1.188E5		
	Sectionwise dP (Pa)	Vortex	dP (Pa)	fraction (%)	Vortex	dP (Pa)	fraction (%)
		F1,F2	8.900E2	1.7	B1,B2	8.699E4	73.2
		F3,F4	1.790E3	3.4	B3	1.174E4	9.9
		F5	4.646E4	87.3	B4	6.140E3	5.2
	Di	2.23					
k-w	**Total dP (Pa)**	1.008E5			2.146E5		
	Sectionwise dP (Pa)	Vortex	dP (Pa)	fraction (%)	Vortex	dP (Pa)	fraction (%)
		F1,F2	7.000E2	0.7	B1,B2	1.501E5	70.0
		F3,F4	1.800E3	1.8	B3	1.819E4	8.5
		F5	9.799E4	97.2	B4	3.710E4	17.3
	Di	2.13					
SST	**Total dP (Pa)**	1.007E5			2.115E5		
	Sectionwise dP (Pa)	Vortex	dP (Pa)	fraction (%)	Vortex	dP (Pa)	fraction (%)
		F1,F2	6.000E2	0.6	B1,B2	1.47E5	69.3
		F3,F4	1.600E3	1.6	B3	1.54E4	7.3
		F5	9.779E4	97.1	B4	4.38E4	20.7
	Di	2.10					

Table 4. 11 Type of vortex (Optimum design B, Re=1E5, SST model, entrance/exit length=10D)

Forward flow		Backward flow	
Vortex	Type	Vortex	Type
F1	Wake	B1	Corner
F2	Wake	B2	Wake
F3	Wake	B3	Wake
F4	Cavity	B4	Wake
F5	Corner	B5	Wake
F6	Wake	B6	Corner
F7	Wake	B7	Wake
F8	Cavity	B8	Wake
F9	Cavity	B9	Wake
F10	Cavity	B10	Wake
F11	Corner	B11	Corner
F12	Wake	B12	Wake
-	-	B13	Wake

Table 4. 12 Effects of each vortex on pressure drop (Optimum design B, Re=1E5, SST model, entrance/exit length=10D)

Optimum design B							
Turbulence model		**Forward flow**			**Backward flow**		
SST	**Total dP (Pa)**	2.997E4			1.317E5		
	Sectionwise dP (Pa)	Vortex	dP (Pa)	fraction (%)	Vortex	dP (Pa)	fraction (%)
		F1-F3	3.030E3	10.1	B1	5.013E4	38.1
		F4,F5	2.190E3	7.3	B2-B4	2.621E4	19.9
		F6,F7	-2.200E2	-0.7	B5,B6	8.790E3	6.7
		F8-F11	1.294E4	43.2	B7-B9	2.873E4	21.8
		F12	9.670E3	32.3	B10-B13	1.367E4	10.4
	Di	4.39					

Table 4. 13 Effects of each vortex on pressure drop (Optimum design B, Re=1E4, entrance/exit length=0D)

Optimum design B							
Turbulence model		**Forward flow**			**Backward flow**		
k-e	**Total dP (Pa)**	4.301E2			1.480E3		
	Sectionwise dP (Pa)	Vortex	dP (Pa)	fraction (%)	Vortex	dP (Pa)	fraction (%)
		F1-F4	3.080E1	7.2	B1	6.512E2	44.0
		F5-F7	2.310E1	5.4	B1-B3	2.283E2	15.4
		F8,F9	3.600E0	0.8	B4,B5	1.747E2	11.8
		F10-F13	1.159E2	26.9	B6	2.882E2	19.5
		F14	2.609E2	60.7	B7-B10	1.371E2	9.3
	Di	3.44					
k-w	**Total dP (Pa)**	3.876E2			1.498E3		
	Sectionwise dP (Pa)	Vortex	dP (Pa)	fraction (%)	Vortex	dP (Pa)	fraction (%)
		F1-F4	3.140E1	8.1	B1	6.404E2	42.7
		F5-F7	2.640E1	6.8	B1-B3	2.088E2	13.9
		F8,F9	-2.000E-1	-0.1	B4,B5	1.085E2	7.2
		F10-F13	1.434E2	37.0	B6	4.178E2	27.9
		F14	1.888E2	48.7	B7-B10	1.226E2	8.2
	Di	3.87					
SST	**Total dP (Pa)**	3.918E2			1.492E3		
	Sectionwise dP (Pa)	Vortex	dP (Pa)	fraction (%)	Vortex	dP (Pa)	fraction (%)
		F1-F4	3.150E1	8.0	B1	6.398E2	42.9
		F5-F7	2.650E1	6.8	B1-B3	1.933E2	13.0
		F8,F9	-2.000E-1	-0.1	B4,B5	1.081E2	7.2
		F10-F13	1.433E2	36.6	B6	4.339E2	29.1
		F14	1.929E2	49.2	B7-B10	1.165E2	7.8
	Di	3.81					

Table 4. 14 Effects of each vortex on pressure drop (Optimum design B, Re=1E4, entrance/exit length=10D)

Optimum design B							
Turbulence model		**Forward flow**			**Backward flow**		
k-e	**Total dP (Pa)**	3.886E2			1.455E3		
	Sectionwise dP (Pa)	Vortex	dP (Pa)	fraction (%)	Vortex	dP (Pa)	fraction (%)
		F1-F3	3.270E1	8.4	B1	5.961E2	41.0
		F4,F5	2.460E1	6.3	B2-B4	1.923E2	13.2
		F6,F7	3.300E0	0.8	B5,B6	1.720E2	11.8
		F8-F11	1.164E2	30.0	B7-B9	2.877E2	19.8
		F12	1.607E2	41.4	B10-B13	1.375E2	9.5
	Di	3.74					
k-w	**Total dP (Pa)**	3.700E2			1.393E3		
	Sectionwise dP (Pa)	Vortex	dP (Pa)	fraction (%)	Vortex	dP (Pa)	fraction (%)
		F1-F3	3.050E1	8.2	B1	5.049E2	36.3
		F4,F5	2.510E1	6.8	B2-B4	2.726E2	19.6
		F6,F7	1.000E0	0.3	B5,B6	7.100E1	5.1
		F8-F11	1.424E2	38.5	B7-B9	3.389E2	24.3
		F12	9.910E1	26.8	B10-B13	1.165E2	8.4
	Di	3.76					
SST	**Total dP (Pa)**	3.499E2			1.378E3		
	Sectionwise dP (Pa)	Vortex	dP (Pa)	fraction (%)	Vortex	dP (Pa)	fraction (%)
		F1-F3	3.070E1	8.8	B1	4.927E2	35.8
		F4,F5	2.510E1	7.2	B2-B4	2.792E2	20.3
		F6,F7	-1.000E-1	0.0	B5,B6	5.860E1	4.3
		F8-F11	1.426E2	40.8	B7-B9	3.542E2	25.7
		F12	8.380E1	23.9	B10-B13	1.093E2	7.9
	Di	3.94					

Table 4. 15 Effects of each vortex on pressure drop (Optimum design B, Re=5E4, entrance/exit length=0D)

Optimum design B							
Turbulence model		**Forward flow**			**Backward flow**		
k-e	**Total dP (Pa)**	1.011E4			3.926E4		
	Sectionwise dP (Pa)	Vortex	dP (Pa)	fraction (%)	Vortex	dP (Pa)	fraction (%)
		F1-F4	7.400E2	7.3	B1	1.623E4	41.3
		F5-F7	5.000E2	4.9	B1-B3	6.220E3	15.8
		F8,F9	5.000E1	0.5	B4,B5	4.500E3	11.5
		F10-F13	2.750E3	27.2	B6	8.563E3	21.8
		F14	6.198E3	61.3	B7-B10	3.746E3	9.5
	Di	3.88					
k-w	**Total dP (Pa)**	9.590E3			3.893E4		
	Sectionwise dP (Pa)	Vortex	dP (Pa)	fraction (%)	Vortex	dP (Pa)	fraction (%)
		F1-F4	7.500E2	7.8	B1	1.634E4	42.0
		F5-F7	6.100E2	6.4	B1-B3	5.860E3	15.1
		F8,F9	-3.000E1	-0.3	B4,B5	3.460E3	8.9
		F10-F13	3.340E3	34.8	B6	9.449E3	24.3
		F14	5.110E3	53.3	B7-B10	3.825E3	9.8
	Di	4.06					
SST	**Total dP (Pa)**	9.469E3			3.845E4		
	Sectionwise dP (Pa)	Vortex	dP (Pa)	fraction (%)	Vortex	dP (Pa)	fraction (%)
		F1-F4	7.800E2	8.2	B1	1.663E4	43.2
		F5-F7	5.900E2	6.2	B1-B3	5.600E3	14.6
		F8,F9	-3.000E1	-0.3	B4,B5	3.720E3	9.7
		F10-F13	3.350E3	35.4	B6	8.873E3	23.1
		F14	4.949E3	52.3	B7-B10	3.630E3	9.4
	Di	4.06					

Table 4. 16 Effects of each vortex on pressure drop (Optimum design B, Re=5E4, entrance/exit length=10D)

Optimum design B							
Turbulence model		**Forward flow**			**Backward flow**		
k-e	**Total dP (Pa)**	8.618E3			3.788E4		
	Sectionwise dP (Pa)	Vortex	dP (Pa)	fraction (%)	Vortex	dP (Pa)	fraction (%)
		F1-F3	7.730E2	9.0	B1	1.467E4	38.7
		F4,F5	5.500E2	6.4	B2-B4	4.640E3	12.2
		F6,F7	4.400E1	0.5	B5,B6	4.090E3	10.8
		F8-F11	2.774E3	32.2	B7-B9	9.136E3	24.1
		F12	3.552E3	41.2	B10-B13	4.039E3	10.7
	Di	4.40					
k-w	**Total dP (Pa)**	8.287E3			3.461E4		
	Sectionwise dP (Pa)	Vortex	dP (Pa)	fraction (%)	Vortex	dP (Pa)	fraction (%)
		F1-F3	7.570E2	9.1	B1	1.290E4	37.3
		F4,F5	5.920E2	7.1	B2-B4	6.770E3	19.6
		F6,F7	-1.500E1	-0.2	B5,B6	2.140E3	6.2
		F8-F11	3.332E3	40.2	B7-B9	8.060E3	23.3
		F12	2.723E3	32.9	B10-B13	3.381E3	9.8
	Di	4.18					
SST	**Total dP (Pa)**	7.709E3			3.349E4		
	Sectionwise dP (Pa)	Vortex	dP (Pa)	fraction (%)	Vortex	dP (Pa)	fraction (%)
		F1-F3	7.390E2	9.6	B1	1.249E4	37.3
		F4,F5	5.740E2	7.4	B2-B4	6.910E3	20.6
		F6,F7	-4.600E1	-0.6	B5,B6	1.740E3	5.2
		F8-F11	3.354E3	43.5	B7-B9	7.905E3	23.6
		F12	2.284E3	29.6	B10-B13	3.207E3	9.6
	Di	4.35					

Table 4. 17 Effects of each vortex on pressure drop (Optimum design B, Re=1E5, entrance/exit length=0D)

Optimum design B							
Turbulence model		**Forward flow**			**Backward flow**		
k-e	**Total dP (Pa)**	4.001E4			1.598E5		
	Sectionwise dP (Pa)	Vortex	dP (Pa)	fraction (%)	Vortex	dP (Pa)	fraction (%)
		F1-F4	3.080E1	7.2	B1	6.490E4	40.6
		F5-F7	2.310E1	5.4	B1-B3	2.283E2	15.4
		F8,F9	3.600E0	0.8	B4,B5	1.747E2	11.8
		F10-F13	1.159E2	26.9	B6	2.882E2	19.5
		F14	2.447E4	61.2	B7-B10	1.371E2	9.3
	Di	4.00					
k-w	**Total dP (Pa)**	3.822E4			1.611E5		
	Sectionwise dP (Pa)	Vortex	dP (Pa)	fraction (%)	Vortex	dP (Pa)	fraction (%)
		F1-F4	3.140E1	8.1	B1	6.510E4	40.4
		F5-F7	2.640E1	6.8	B1-B3	2.088E2	13.9
		F8,F9	-2.000E-1	-0.1	B4,B5	1.085E2	7.2
		F10-F13	1.434E2	37.0	B6	4.178E2	27.9
		F14	2.113E4	55.3	B7-B10	1.226E2	8.2
	Di	4.22					
SST	**Total dP (Pa)**	3.893E4			1.691E5		
	Sectionwise dP (Pa)	Vortex	dP (Pa)	fraction (%)	Vortex	dP (Pa)	fraction (%)
		F1-F4	3.150E1	8.0	B1	6.670E4	39.4
		F5-F7	2.650E1	6.8	B1-B3	1.933E2	13.0
		F8,F9	-2.000E-1	-0.1	B4,B5	1.081E2	7.2
		F10-F13	1.433E2	36.6	B6	4.339E2	29.1
		F14	2.159E4	55.5	B7-B10	1.165E2	7.8
	Di	4.35					

Table 4. 18 Effects of each vortex on pressure drop (Optimum design B, Re=1E5, entrance/exit length=10D)

Optimum design B							
Turbulence model		**Forward flow**			**Backward flow**		
k-e	**Total dP (Pa)**	3.325E4			1.502E5		
	Sectionwise dP (Pa)	Vortex	dP (Pa)	fraction (%)	Vortex	dP (Pa)	fraction (%)
		F1-F3	3.060E3	9.2	B1	5.780E4	38.5
		F4,F5	2.160E3	6.5	B2-B4	1.911E4	12.7
		F6,F7	1.400E2	0.4	B5,B6	1.451E4	9.7
		F8-F11	1.110E4	33.4	B7-B9	3.843E4	25.6
		F12	1.361E4	40.9	B10-B13	1.590E4	10.6
	Di	4.52					
k-w	**Total dP (Pa)**	3.230E4			1.398E5		
	Sectionwise dP (Pa)	Vortex	dP (Pa)	fraction (%)	Vortex	dP (Pa)	fraction (%)
		F1-F3	3.040E3	9.4	B1	5.197E4	37.2
		F4,F5	2.290E3	7.1	B2-B4	2.600E4	18.6
		F6,F7	-9.000E+1	-0.3	B5,B6	9.610E3	6.9
		F8-F11	1.288E4	39.9	B7-B9	3.230E4	23.1
		F12	1.139E4	35.3	B10-B13	1.527E4	10.9
	Di	4.33					
SST	**Total dP (Pa)**	2.997E4			1.317E5		
	Sectionwise dP (Pa)	Vortex	dP (Pa)	fraction (%)	Vortex	dP (Pa)	fraction (%)
		F1-F3	3.030E3	10.1	B1	5.013E4	38.1
		F4,F5	2.190E3	7.3	B2-B4	2.621E4	19.9
		F6,F7	-2.200E2	-0.7	B5,B6	8.790E3	6.7
		F8-F11	1.294E4	43.2	B7-B9	2.873E4	21.8
		F12	9.670E3	32.3	B10-B13	1.367E4	10.4
	Di	4.39					

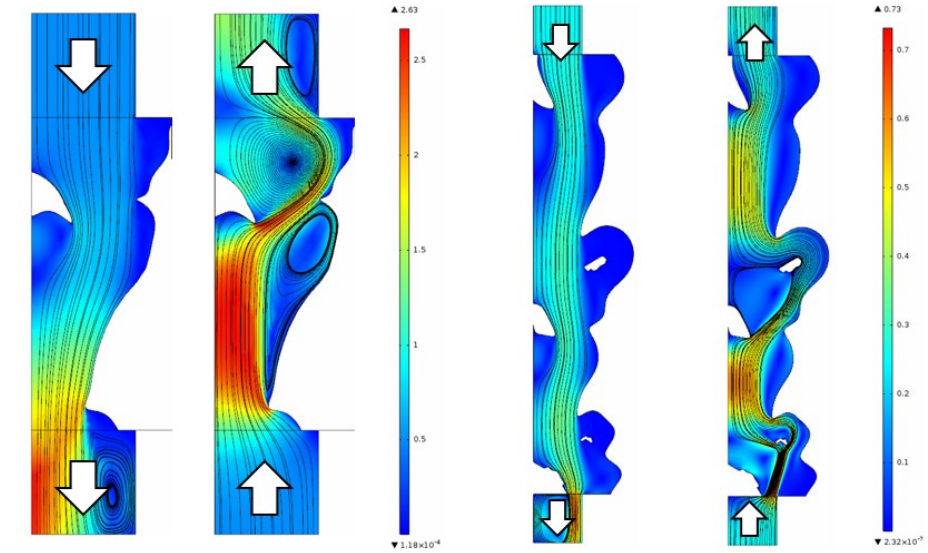

Figure 4. 1 Preliminary performance validation results (Velocity field)

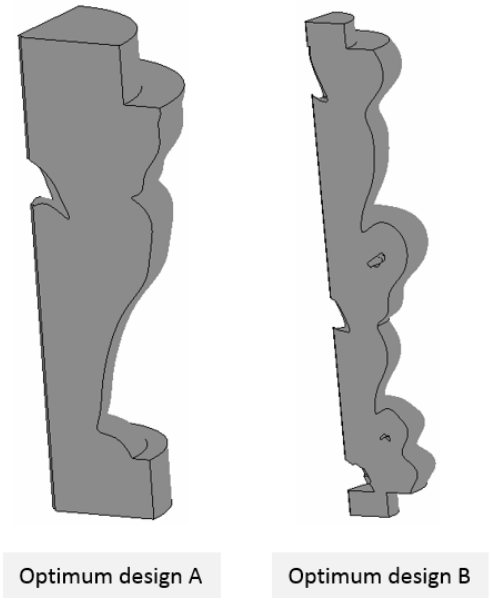

Figure 4. 2 Computational domain for 3-D CFD analysis

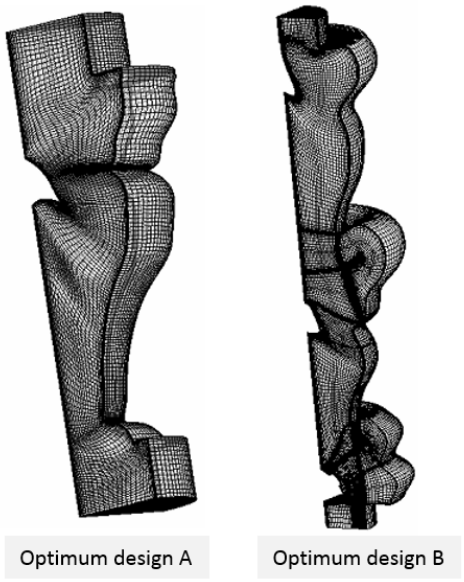

Figure 4. 3 Grid models generated using GRIDGEN

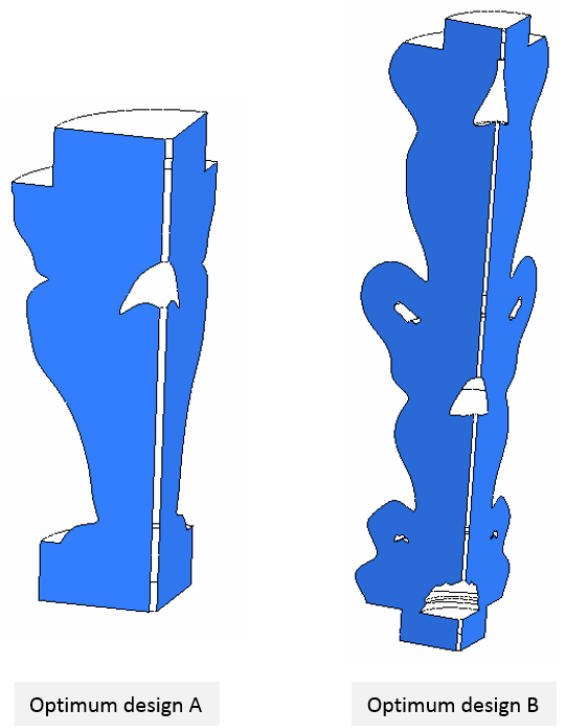

Figure 4. 4 Rotational periodic boundaries

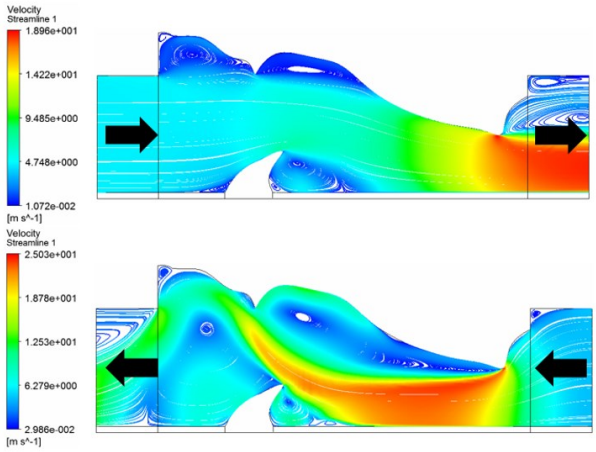

Figure 4. 5 3-D CFD analysis results (Streamline) (Optimum design A, Re=1E5, SST model, entrance/exit length=0D)

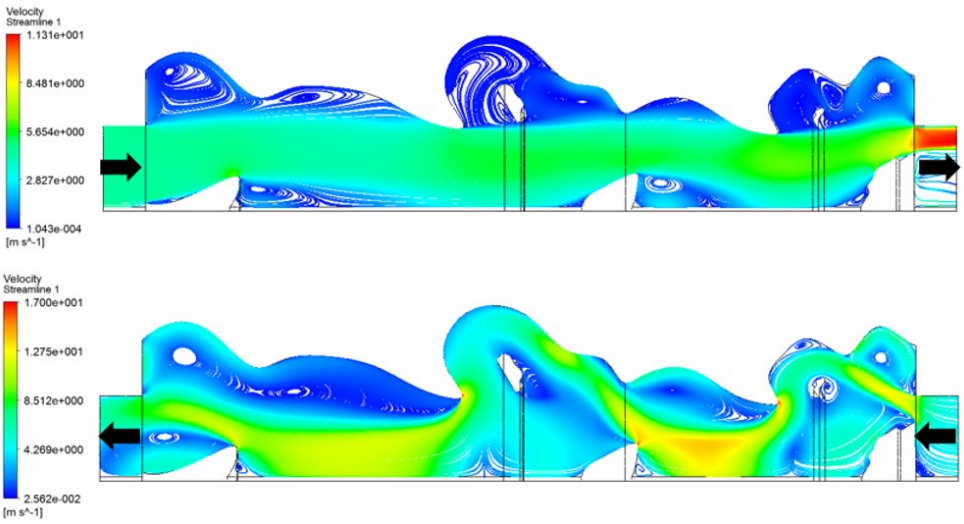

Figure 4. 6 3-D CFD analysis results (Streamline) (Optimum design B, Re=1E5, SST model, entrance/exit length=0D)

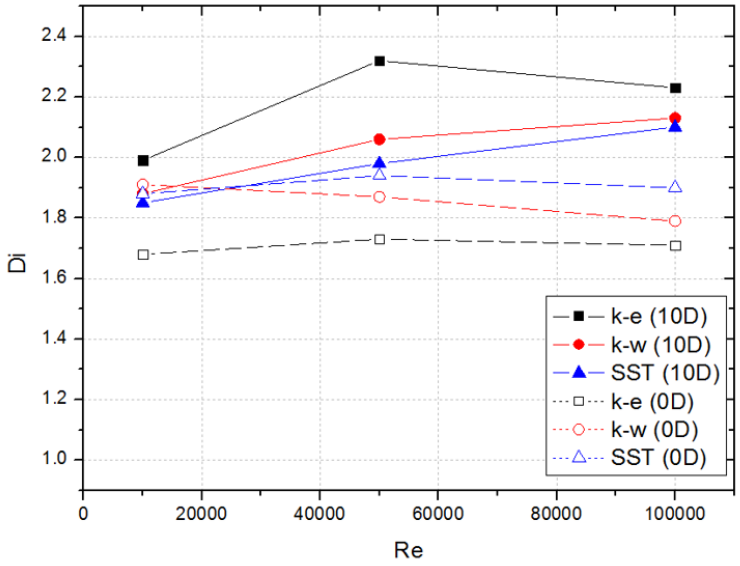

Figure 4. 7 Sensitivity study results (Optimum design A)

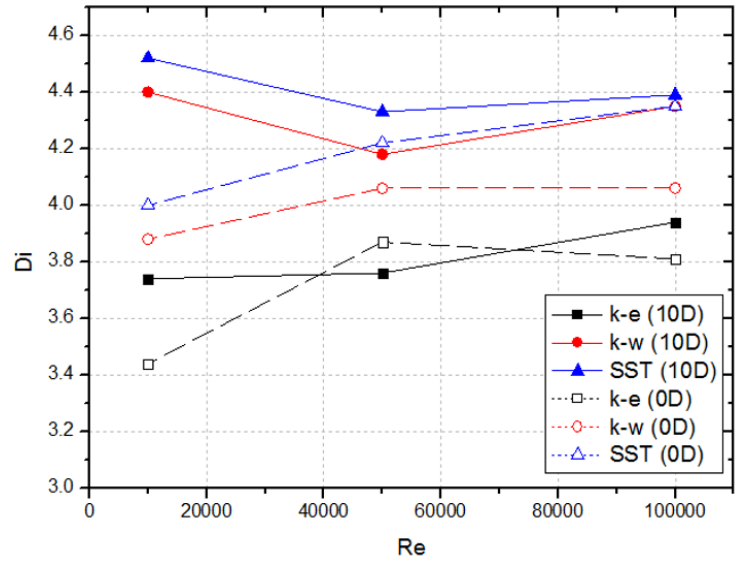

Figure 4. 8 Sensitivity study results (Optimum design B)

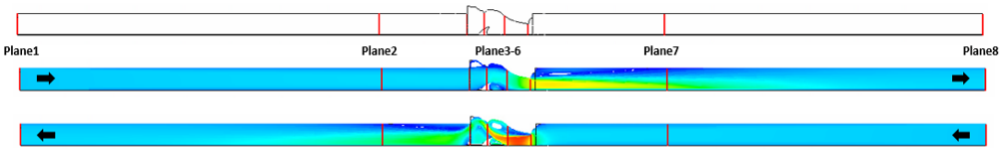

Figure 4. 9 Planes located both sides of vortices (Optimum design A, Re=1E5, SST model, entrance/exit length=10D)

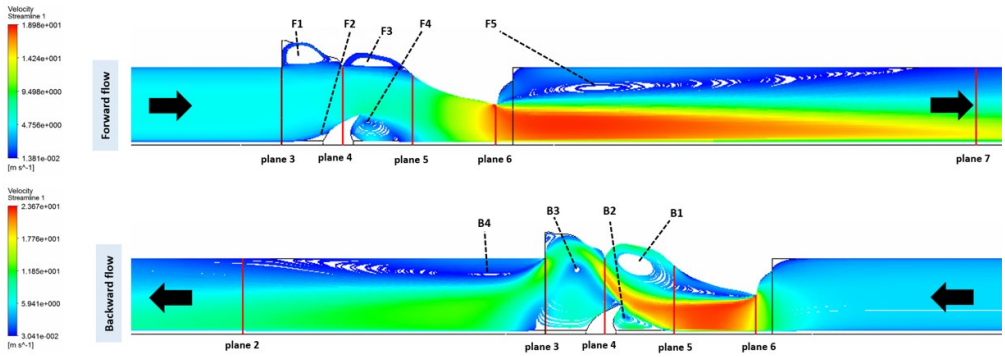

Figure 4. 10 Designation of vortex (Optimum design A, Re=1E5, SST model, entrance/exit length=10D)

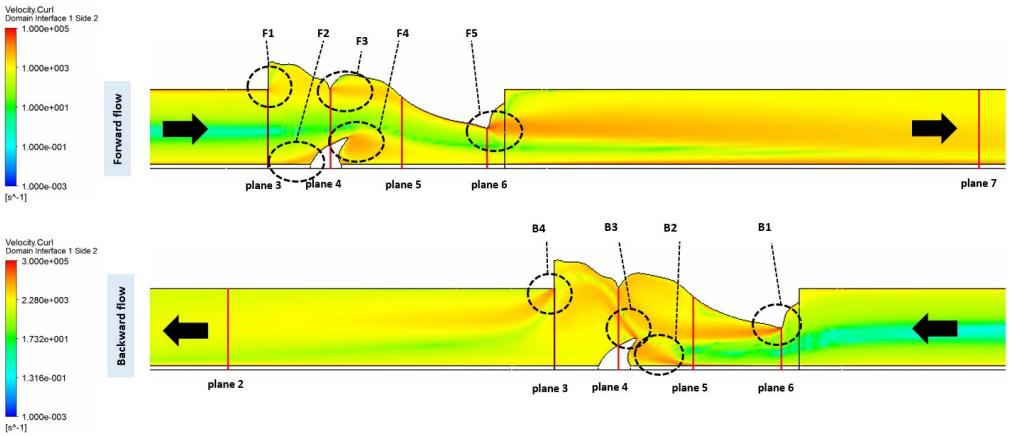

Figure 4. 11 Identification of vortex type (Vorticity field) (Optimum design A, Re=1E5, SST model, entrance/exit length=10D)

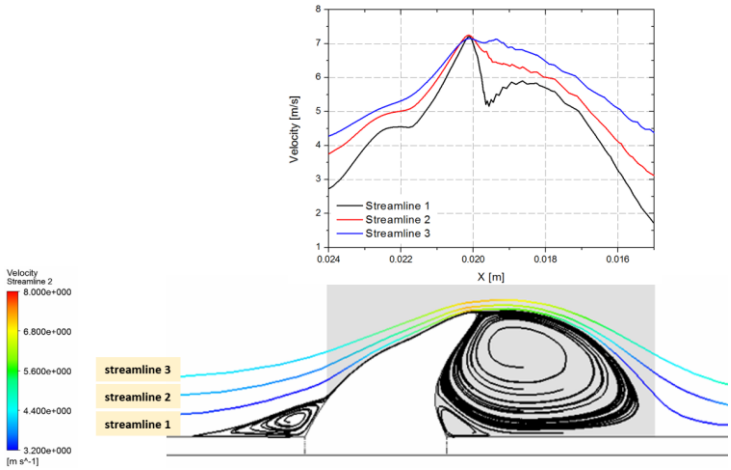

Figure 4. 12 Coanda effect (Optimum design A, Re=1E5, SST model, entrance/exit length=10D)

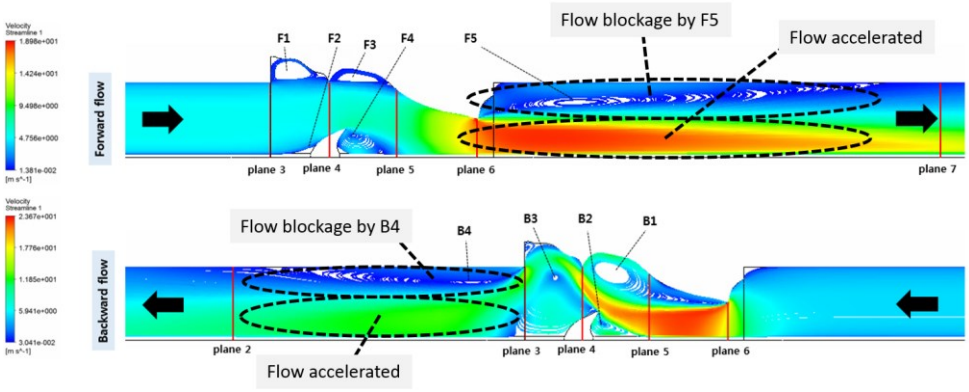

Figure 4. 13 Flow blockage and flow acceleration (Optimum design A, Re=1E5, SST model, entrance/exit length=10D)

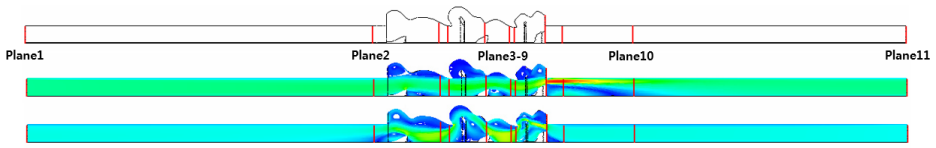

Figure 4. 14 Planes located both sides of vortices (Optimum design B, Re=1E5, SST model, entrance/exit length=10D)

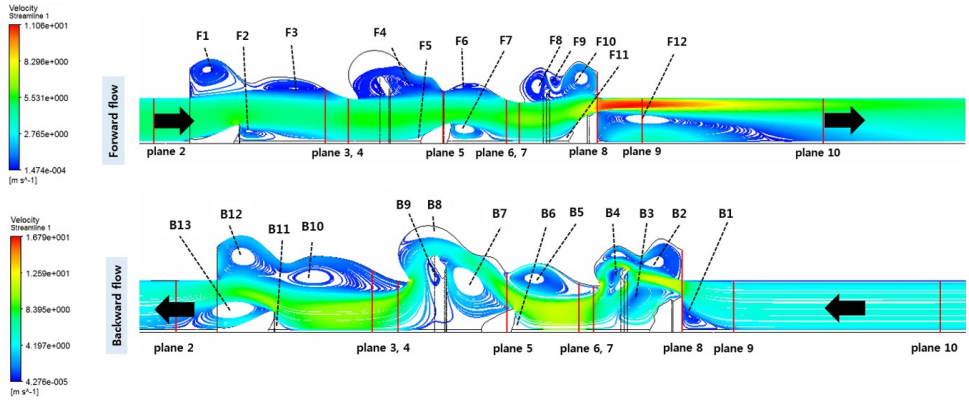

Figure 4. 15 Designation of vortex (Optimum design B, Re=1E5, SST model, entrance/exit length=10D)

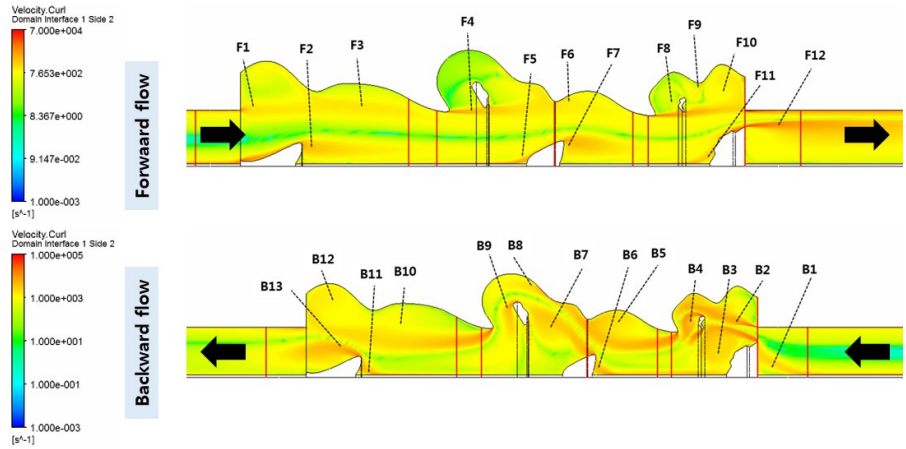

Figure 4. 16 Identification of vortex type (Vorticity field) (Optimum design B, Re=1E5, SST model, entrance/exit length=10D)

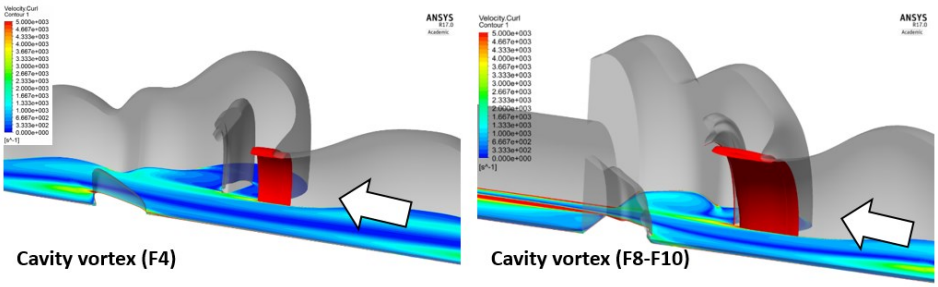

Figure 4. 17 Boundary layer development by cavity vortex (Optimum design B, Re=1E5, SST model, entrance/exit length=10D)

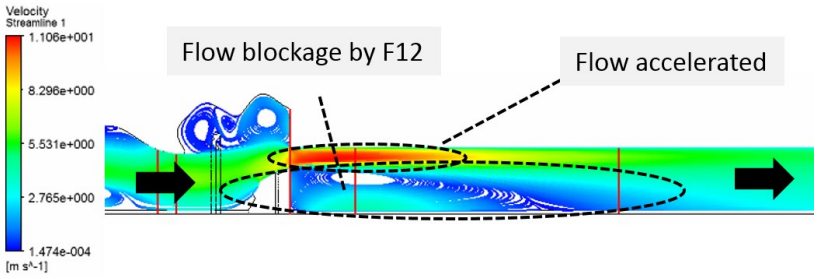

Figure 4. 18 Flow blockage and flow acceleration (Optimum design B, Re=1E5, SST model, entrance/exit length=10D)

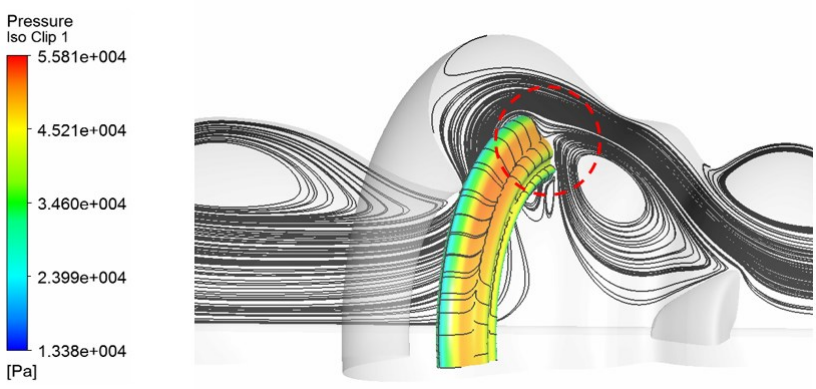

Figure 4. 19 Limiting streamline (Optimum design B, Re=1E5, SST model, entrance/exit length=10D)

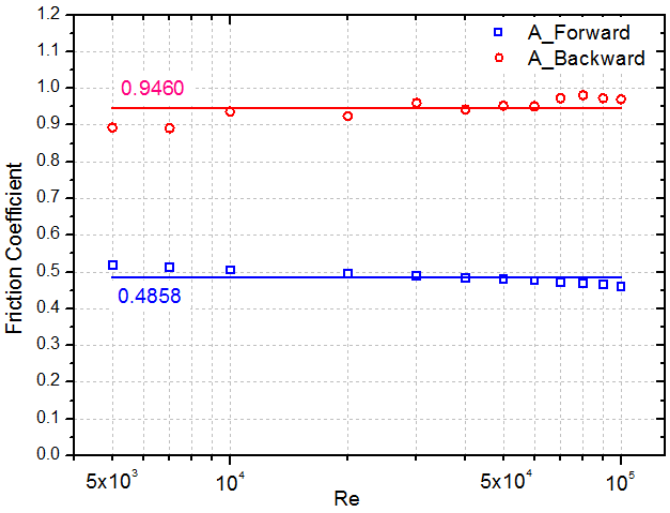

Figure 4. 20 Friction coefficient (Optimum design A, Re=1E5, SST model, entrance/exit length=10D)

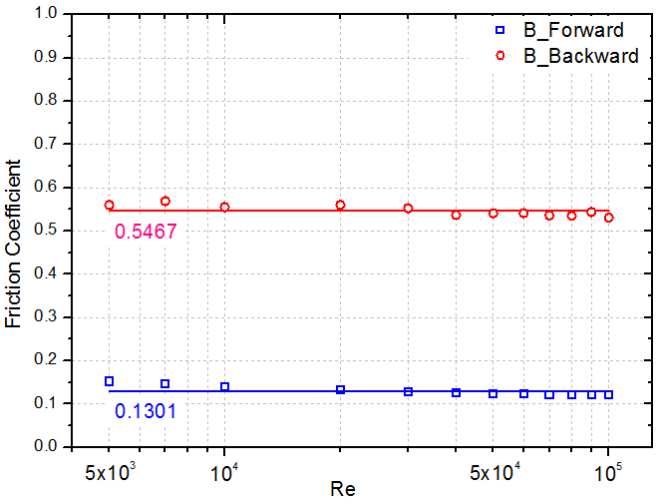

Figure 4. 21 Friction coefficient (Optimum design B, Re=1E5, SST model, entrance/exit length=10D)

Chapter 5

Summary and Conclusions

5.1 Summary

Vortex-type fluidic diode port of hybrid loop-pool SFR is designed with topology optimization and the performance is validated and evaluated using 3-D CFD simulation.

Hybrid loop-pool type SFR was proposed by INL which takes advantage of existing loop type and pool type reactors. In this system, flow rate and direction is changed according to operation mode by passive flow control device, fluidic diode. To achieve enhanced passive safety of the system, study on design improvement of fluidic diode axial port is conducted. In this study, reference fluidic diode is set as vortex-type and performance is defined as diodicity.

Topology optimization is a mathematical method to optimize material distribution in design domain with predefined boundary condition. It is appropriate for getting a conceptual design at the initial stage of design process. With the purpose of simplification, 2-D axisymmetric domain is selected for axial port design. For numerical stability and quality of topology optimization results, a new parameter is derived and set as objective function. In this study, topology optimization has been conducted on parametric cases to identify the effects of

Reynolds number and aspect ratio. Two designs of high performance are selected as the optimum design for the following design process. As topology optimization is conducted in laminar flow regime, performance is preliminarily validated in turbulent regime using COMSOL CFD. The results show that performance of both designs is greater or the same than the original design value. Since topology optimized designs have small structures and rough wall surfaces that worsen manufacturability, those are removed or simplified based on sensitivity study. By adding supporting structures on 3-D revolved port designs, final port designs are achieved.

Port performance should be validated in detail because (1) final designs have difference with the original designs, (2) there are complicated flow field with strong vortex and (3) COMSOL CFD that used in preliminary performance validation has some limitations on solving high Reynolds turbulent flow. In this study, a quarter of 3-D port design is selected as computational domain. GRIDGEN is used to generate grid model with several iterations to catch vortex structure clearly. CFD-specialized software, ANSYS CFX, is used for 3-D CFD analysis. Sensitivity study is conducted in order to understand effects of turbulence model, Reynolds number, and entrance/exit length. Performance ranges of 10D cases are found to be 1.7~2.3 for port A and 3.7~4.5 for port B in 1×10^4<Re<1×10^5, respectively. Vortex analysis is conducted and it is found that the large vortex generated on the outlet significantly deteriorates performance and can be removed with design modification. The type of each vortex is identified and advanced study is required on analyzing resonance effect of cavity vortex. Physical phenomena such as coanda effect and flow blockage affecting performance and pressure drop are observed. Friction loss coefficient is derived as a constant based on CFD analysis results.

5.2 Recommendations

Through the present study, the following further studies are suggested:

1. Objective function used in topology optimization only considers diodicity, the ratio of forward and backward flow pressure drop. To maintain natural circulation sufficient to remove decay heat during LOFC transients, however, the absolute pressure drop of forward flow should remain low. Appendix C shows the pressure drop of optimized port is relatively high compared to that of straight pipe and thus natural circulation is reduced. Therefore, development and application of objective function in topology optimization has to be studied.
2. The parametric study results of typology optimization show that in the same aspect ratio, even a small change of Reynolds number draws different optimized design because there are many local optimum points. Outer iteration that integrate the result of various Reynolds numbers can give a consistent result for flow between this range. Further work on implementing outer iteration in topology optimization algorithm is strongly suggested.
3. It is found that a large vortex lies on the outlet and seriously deteriorates port performance. This is due to sudden expansion of flow area which is not intended in topology optimization stage. Even adding a smooth diffuser would significantly enhance port performance. Design modification on the outlet has to be studied in more detail.
4. Cavity vortex is observed in the backward flow of passing optimum design

B. It has the possibility of causing resonance effects and thus decreasing structural integrity. Further work on the resonance effect of cavity vortex can be meaningful.

5. The designed port performance is only numerically validated. Experiments on optimized port designs and on the overall part including vortex-type fluidic diode and optimized ports are essential for performance validation. Further work on the validation experiment is strongly suggested.

Nomenclature

D	Diameter (m)
Da	Darcy number
Di	Diodicity
E	Energy dissipation rate (W m^{-3})
f_A	Friction loss coefficient of optimum design A
f_B	Friction loss coefficient of optimum design B
L	Length of design domain (m)
L_{ent}	Length of entrance region (m)
p	Convexity control parameter in SIMP
P	Pressure (Pa)
$P*$	Dimensionless pressure
q	Convexity control parameter in Brinkman penalization
r_{ent}	Radius of entrance region (m)
R	Radius of design domain (m)
$\boldsymbol{R}$	Constraints of topology optimization
t	Time (s)
$t*$	Dimensionless time
$\bar{u}$	Flow velocity (m s^{-1})
$\bar{u}*$	Dimensionless flow velocity (m s^{-1})
u_r	Radial component of flow velocity (m s^{-1})
u_z	Axial component of flow velocity (m s^{-1})
y^+	Dimensionless wall distance
t	Time (s)

s	Flow variable
V	Total volume of material (m^3)

Greek Letters

α	Degree of impermeability (kg s^{-1} m^{-3})
α_L	Lower limit of degree of impermeability (kg s^{-1} m^{-3})
α_U	Upper limit of degree of impermeability (kg s^{-1} m^{-3})
γ	Density function
ΔP	Pressure drop (Pa)
ε	Optimization convergence residual criteria
κ	Permeability (m^2)
λ	Adjoint variable
μ	Viscosity (Pa s)
ρ	Density (kg m^{-3})
Φ	Objective function of topology optimization
Ω	Design domain of topology optimization
$d\Omega$	Design domain boundary of topology optimization

Subscripts

A	Optimum design A
B	Optimum design B

forward	Forward flow passing fluidic diode
backward	Backward flow passing fluidic diode

Superscripts

*	Dimensionless

References

ANSYS, ANSYS CFX-Solver Modeling Guide, Release 15.0, 2013.

ANSYS, ANSYS CFX-Solver Theory Guide, Release 15.0, 2013.

Borrvall, T., Peterson, J., “Topology optimization of fluids in Stokes flow”, International Journal for Numerical Methods in Fluids”, vol. 41, pp. 77-107, 2003.

Chikazawa, Y., Aizawa, K., Shiraishi, T., Sakata, H., “Experimental Demonstration of Flow Diodes Applicable to a Passive Decay Heat Removal System for Sodium-Cooled Reactors”, Jounal of Nuclear Science and Technology, vol. 46, pp. 321-330, 2009.

COMSOL, COMSOL Multiphysics CFD Module User’s Guide, Ver. 5.1, 2015.

Holcomb, D. E., Cetiner, S. M., Flanagan, G. F., Peretz, F. J., Yoder, Jr., G. L., “An Analysis of Testing Requirements for Fluoride Salt-Cooled High Temperature Reactor Components”, ORNL/TM-2009/297, Oak Ridge National Laboratory, 2009.

Kulkarni, A. A., Ranade, V. V., Rajeev, R., Koganti, S. B., “CFD Simulation of Flow in Vortex Diodes”, AIChE Journal, vol. 54, pp. 1139-1152, 2008.

Lee, K., “Topology Optimization of Convective Cooling System Designs”,

Ph.D. thesis, University of Michigan, 2012.

Lin, S., Zhao, L., Guest, J. K., Weihs, T. P., Liu, Z., “Topology Optimization of Fixed-Geometry Fluid Diodes”, Journal of Mechanical Design, vol. 137, 2015.

Okkels, F., Bruus, H., “Scaling behavior of optimally structured catalytic microfluidic reactors”, Physical Review, vol. 75, 2007.

Othmer, C., Kaminski, T., Giering, R., “Computation of Topological Sensitivities in Fluid Dynamics: Cost Function Verstility”, European Conference on Computational Fluid Dynamics, Egmond aan Zee, Netherlands, 2006.

Pointwise, Gridgen Tutorial Workbook, Version 15, 2006.

Rajasekaran, J., “On the flow characteritics behind a backward-facing step and the design of a new axisymmetric model for their study”, Master’s thesis, University of Toronto, 2011.

Yoder, Jr., G. L., Elkassabgi, Y., Leon, G. D., Fetterly, C., Ramos, J., Robbins, J., Cunningham, R. B., “Vortex Diode Analysis and Testing for Fluoride Salt-Cooled High-Temperature Reactors”, ORNL/TM-2011/425, Oak Ridge National Laboratory, 2011.

Zhang, H., Zhao, H., Davis, C., Memmott, M., “RELAP5 Analysis of the Hybrid Loop-Pool Design for Sodium Cooled Fast Reactors”, International

Congress on Advances in Nuclear Power Plants (ICAPP 2008), Anaheim, California, USA, 2008.

Zhao, H., Zhang, H., Mousseau, V. A., Peterson, P. F., “Improving SFR Economics Through Innovations from Thermal Design and Analysis Aspects”, International Congress on Advances in Nuclear Power Plants (ICAPP 2008), Anaheim, California, USA, 2008.

Appendix A

Derivation of Objective Function

Assuming steady and adiabatic state,

$h_{in} = h_{out}$ and $dh = 0$

Entropy generation rate in the system,

$$\dot{S_{gen}} = \dot{m}(s_{out} - s_{in})$$

For any pure substance,

$dh = Tds + vdP = 0$,

therefore

$$ds = -\frac{vdP}{T}$$

and entropy generation rate is as follows.

$$\therefore \dot{S_{gen}} = \dot{m}\left(\int_{P_{out}}^{P_{in}} \frac{v}{T} dP\right)_{h=const}$$

For incompressible fluid ($c = c_p = c_v,\ \rho$),

$$dh = c_p dT + v(1 - \alpha T)dP = cdT + vdP = 0$$

Therefore,

$$vdP = -cdT$$

$$v(P_{in} - P_{out}) = c(T_{out} - T_{in})$$

$$v\Delta P = c\Delta T$$

$$\Delta T = \frac{v}{c}\Delta P = \frac{\Delta P}{\rho c}$$

Thus

$$\therefore \dot{S_{gen}} = \dot{m}c\, ln\frac{T_{out}}{T_{in}} = \dot{m}c\, ln\frac{T_{in}+\Delta T}{T_{in}} = \dot{m}c\, ln\left(1+\frac{\Delta T}{T_{in}}\right) = \dot{m}c\, ln\left(1+\frac{\Delta P}{\rho c T_{in}}\right)$$

If $\Delta P \ll \rho c T_{in}$,

$$\therefore \dot{S_{gen}} \approx \frac{\dot{m}\Delta P}{\rho T_{in}} = \frac{Q\Delta P}{T_{in}}$$

Viscous dissipation rate in the system is represented with pressure drop,

$$E_{diss} = \dot{m}[(h - T_0 s)_{in} - (h - T_0 s)_{out}] = T_0 \dot{S_{gen}} = Q\Delta P$$

Therefore, the ratio of power dissipation rate is equal to 1/Di,

$$\frac{E_{diss,\,backward}}{E_{diss,forward}} = \frac{(Q\Delta P)_f}{(Q\Delta P)_b} = \frac{\Delta P_f}{\Delta P_b} = \frac{1}{\mathrm{Di}}$$

Appendix B

CFD Validation with Experimental Results of Backward-Facing Step Flow

This section presents the validation of 3-D CFD analysis results in view of reattachment length in backward-facing step (BFS) flow.

Physics in BFS flow is summarized in Fig B.1. A similar phenomena is observed at the outlet of forward flow in optimum design A as seen in Fig B.2. In this study, reattachment length (x_R) is selected as a parameter to determine the accuracy of CFD analysis.

Most of experiments have been conducted in planar backward-facing step geometry as seen in Fig B.3. There are five flow parameters affecting reattachment length according to previous study (Rajasekaran, 2011); (1) Aspect ratio (w/H), (2) Expansion ratio (Y_1/Y_2), (3) Free stream turbulence intensity ($\sqrt{u'^2 + v'^2 + w'^2}/U_\infty$), (4) Reynolds number ($Re_H$), and (5) Boundary layer thickness (δ) at separation. Aspect ratio cannot be defined in this study because CFD analysis is conducted on 2-D axisymmetric port geometry. Free stream turbulence intensity is found to be negligible compared to other parameters. And boundary layer thickness gives small contribution compared to expansion ratio and Reynolds number. In this study, expansion ratio, Reynolds number, and boundary layer thickness are used for validation.

The effects of flow parameters on reattachment length is as follows according

to previous study (Rajasekaran, 2011); (1) Reattachment length increases as expansion ratio increases, (2) Reattachment length increases as Reynolds number increases, and (3) Reattachment length decreases as boundary layer thickness increases.

Flow parameters of BFS flow in a certain case of CFD analysis are displayed in Table B.1. These are compared with experimental results summarized in previous study (Rajasekaran, 2011). Fig B.4 shows reattachment length with regard to Expansion ratio and expansion ratio of CFD analysis is marked as a red line. Fig B.5 and Fig B.6 show reattachment length with regard to Reynolds number and boundary layer thickness, respectively, with a red line representing CFD analysis result. Reynolds number and expansion ratio of this study are very high compared to those of experimental condition. Although the conditions are not within the range, it is identified that CFD results follow the general trend aforementioned. Relatively long reattachment length is the result of high expansion ratio, high Reynolds number, and low-to-moderate boundary layer thickness which gives only small contribution.

CFD analysis is well validated with existing experimental data, however, there are some limitations as follows; (1) The CFD result is compared with flat-backward-facing step experiment data because there is little data obtained from an axisymmetric geometry, and (2) Experimental data was obtained for the fully-developed turbulent flow at separation while that condition was not met in CFD result due to sudden flow area decrease.

Table B. 1 Flow parameters of BFS flow in CFD analysis (optimum design A, Forward flow, SST model, 10D)

$\mathbf{Re_H \times 10^4}$	$\mathbf{Y_1/Y_2}$	$\boldsymbol{\delta}$**/H**	$\sqrt{u'^2 + v'^2 + w'^2}/U_\infty$	$\mathbf{x_R/H}$
9.2	1.94	0.648	0.2	11.21

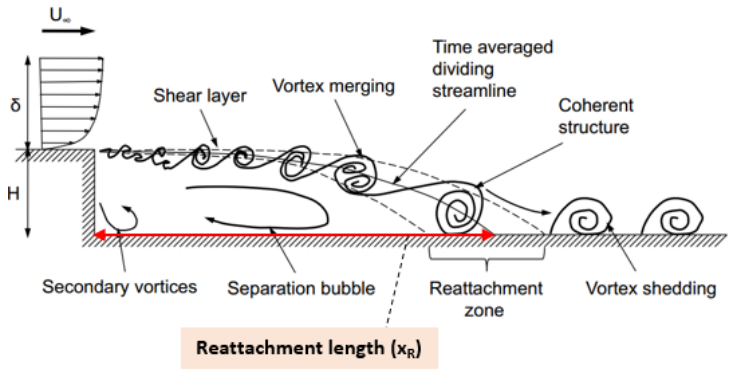

Figure B. 1 Physical phenomena shown in BFS flow

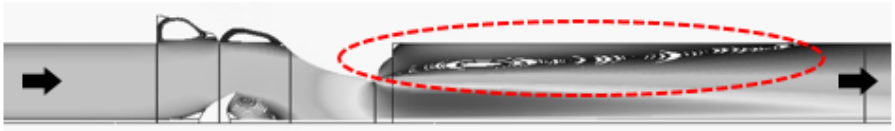

Figure B. 2 BFS flow generated in forward flow of optimum design A (Streamline)

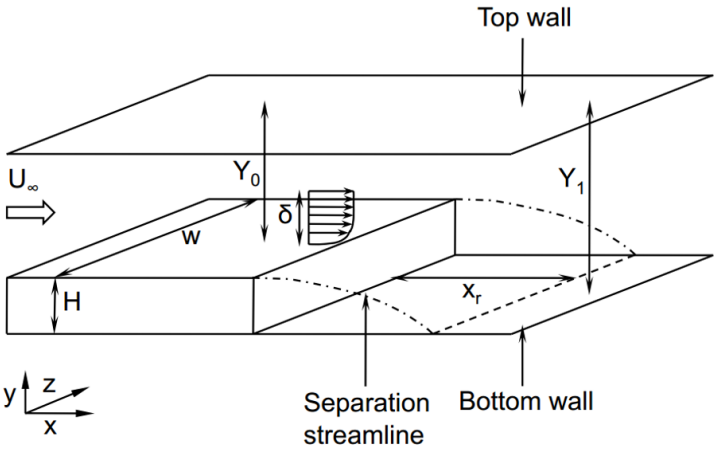

Figure B. 3 Planar backward-facing step geometry (Rajasekaran, 2011)

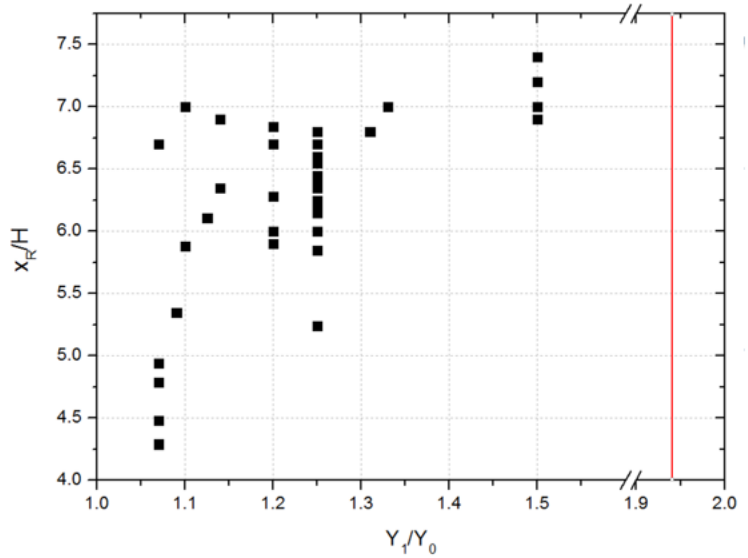

Figure B. 4 Normalized reattachment length (x_R/H) with regard to expansion ratio (Y_1/Y_2)

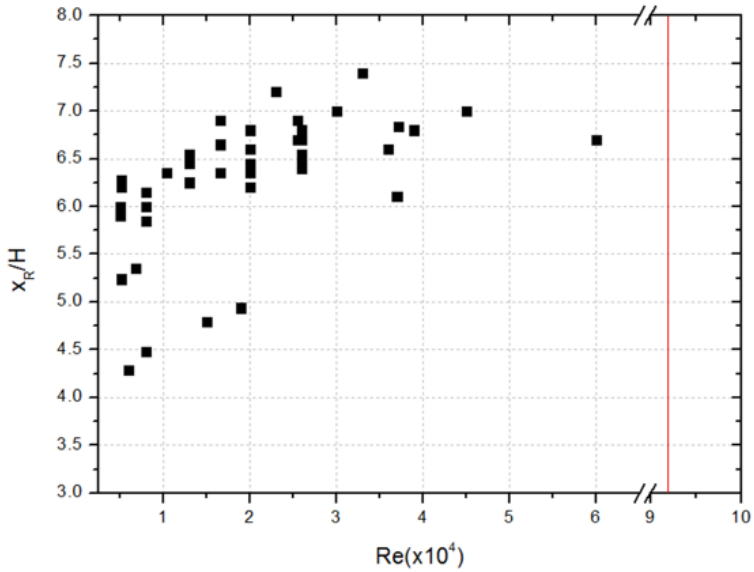

Figure B. 5 Normalized reattachment length (x_R/H) with regard to Reynolds number ($Re_H\ /10^4$)

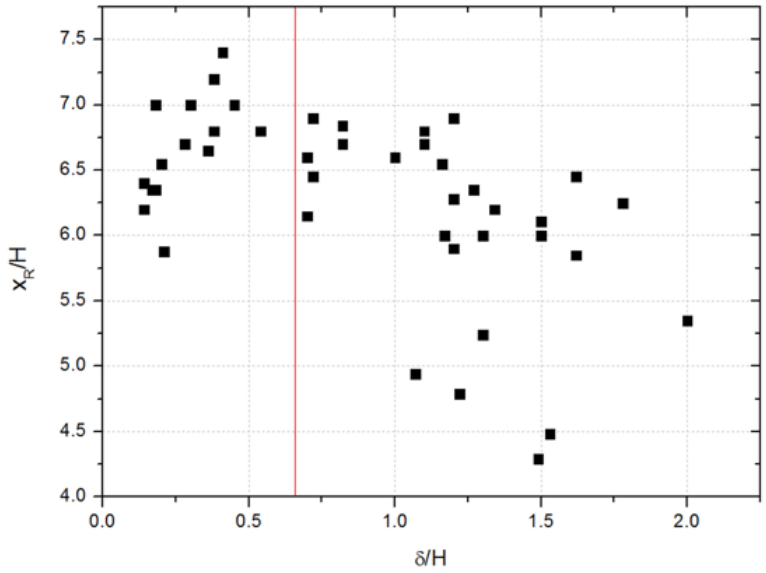

Figure B. 6 Normalized reattachment length (x_R/H) with regard to normalized boundary layer thickness (δ/H)

Appendix C

Comparison of Pressure Loss of Flow Passing Straight Pipe and Optimized Port Design

This section presents the comparison of pressure drop of each flow passing straight pipe and optimized port design.

The objective function used in topology optimization only considers diodicity, the ratio of forward and backward flow pressure drop. However, for natural circulation to be sufficient to remove decay heat during LOFC transients, the absolute pressure drop of forward flow should remain low level.

In order to identify how much forward flow pressure drop passing the optimized design increases compared to that of straight pipe, numerical simulation on straight pipe flow is conducted using COMSOL CFD. The pipe diameter, length, boundary conditions and turbulent model are set as those of port flow. The results are shown in Table C.1. In turbulent regime of 1E4<Re<1E5, pressure drop of port A and B is 13~24 times and 4~6 times that of straight pipe, respectively.

This increase in forward flow pressure drop can reduce the cooling ability by natural circulation. As it is found that 90~97% and 23~32% of forward and backward pressure drop is generated by the large vortex on the outlet and it can be significantly reduced by design modification, it is expected that optimized port design gives sufficiently low forward pressure drop.

Table C. 2 Pressure drop of straight pipe and optimized port design (Forward flow, SST model, entrance/exit length=10D)

Optimum design	Re	Pressure drop (Pa)		Ratio (P2/P1)
		Straight pipe (P1)	Port (P2)	
A	1E4	8.259E1	1.305E3	13.4
	5E4	1.268E3	2.622E4	20.7
	1E5	4.229E3	1.077E5	23.8
B	1E4	9.083E1	3.499E2	3.85
	5E4	1.401E3	7.709E3	5.50
	1E5	4.676E3	2.997E4	6.41

국문 초록

소듐냉각고속로는 현재 연구가 진행되고 있는 대표적인 4세대 원전으로 계통의 형태에 따라 크게 루프형과 풀형으로 구분되며 최근에는 루프형과 풀형의 구조를 결합하여 안전성과 경제성이 향상된 하이브리드 루프-풀형 원자로가 제안되었다. 하이브리드 노형의 1차 계통에는 피동 유량 제어 장치인 Fluidic diode가 설치되어 있어, 정상운전 및 사고상태에 따라 유량 및 노심 열제거량을 피동적으로 조절한다. 따라서 Fluidic diode의 성능을 대표하는 Diodicity는 하이브리드 노형의 피동안전성을 확보하고 효율 손실을 최소화 하기 위해서 되도록 높게 유지되어야 하는 것이 중요하다. Vortex-type fluidic diode는 기존에 제안된 Fluidic diode 중 하나로, 본 연구에서는 위상최적화를 이용한 축방향 포트의 설계를 통해서 Fluidic Diode의 전체적인 성능을 향상시킬 수 있는 방안에 대해서 연구를 수행하였다.

위상최적화는 경계 조건이 주어진 설계 영역 내의 물질 분포를 최적화하는 수학적 방법으로, 목적함수를 최소화시키는 설계 변수를 도출한다. 위상최적화에서는 설계 변수로 밀도함수를 사용하는데, 이것은 각 격자마다 값이 정해지며 0 (고체 영역) 이상 1 (유체 영역) 이하의 연속적인 분포를 갖는다. 운동량 방정식에 다아시(Darcy) 마찰력 항을 추가함으로써, 유체, 고체 및 중간 영역의 유동을 하나의 방정식으로 풀 수 있다. 본 연구에서는 수치적 안정성과 위상최적화 결과 향상을 위해 Diodicity를 대체하는 새로운 목적함수를 유도하였다.

본 연구에서는 축방향 포트의 위상최적화 설계를 위해 2-D 축대칭 영역을 해석 영역으로 설정하였다. 다양한 레이놀즈수와 종횡비에 대해 위상최적화를 수행하였으며, 성능이 가장 높은 두 형상을 최적 설계로 선정하였다. 현재 유동해석을 위한 위상최적화는 층류영역에 주로 한정되어 있으며 따라서 본 연구에서도 층류 영역에서의 위상최적화를 적용하였다. 하지만 층류영역에서 높은 Diodicity를 가지는 포트는 난류영역에서도 높은 Diodicity를 가질 것으로 가정할 수 있으며, 이것을 검증하기 위해서 층류영역에서 얻어진 최적화 형상을 단순한 COMSOL CFD 모델에 적용하여 난류 영역에서 검증을 수행하였다. 그 결과 난류 영역에서의 성능은 층류에서 얻어진 성능과 동일하거나 더 큰 것으로 확인되었다. 포트의 실제 제작성을 저하시키는 요인을 줄이기 위해 Smoothing과 Trimming을 통해 형상을 단순화하였고, 중심/주변부 구조물을 고정하기 위한 지지대를 추가하여 최종 설계를 도출하였다.

최종 설계안에 대한 유동학적 특성을 살펴보고 정확한 성능검증 및 평가를 위해서 3차원 전산유체해석(CFD)을 수행하였다. 격자 모델 구성과 CFD 해석에는 각각 GRIDGEN과 ANSYS CFX가 사용되었다. 난류모델, 레이놀즈수, 입출구길이에 따른 영향을 살펴보기 위해 민감도 분석을 수행하였다. 그 결과 포트의 운전조건으로 예상되는 1×10^4 <Re< 1×10^5 영역에서 포트 A와 B의 성능은 각각 1.7~2.3, 3.7~4.5의 범위로 확인되었다. 각 와류에 의한 영향을 파악하고, 설계 개선점을 파악하며, 구조와 성능에 미치는 물리적 현상을 파악하기

위해 와류 분석을 수행하였다. 또한 CFD 해석 결과를 바탕으로 각 방향의 유동에 대한 마찰계수를 상수로 유도하였다.

주요어

하이브리드 루프-풀 소듐냉각고속로, 위상최적화, 유동 다이오드, 다이오드 성능변수, 전산유체해석

학번: 2013-21018